Cell

Bacteriophages inhibit and evade cGAS-like immune function in bacteria

Graphical abstract

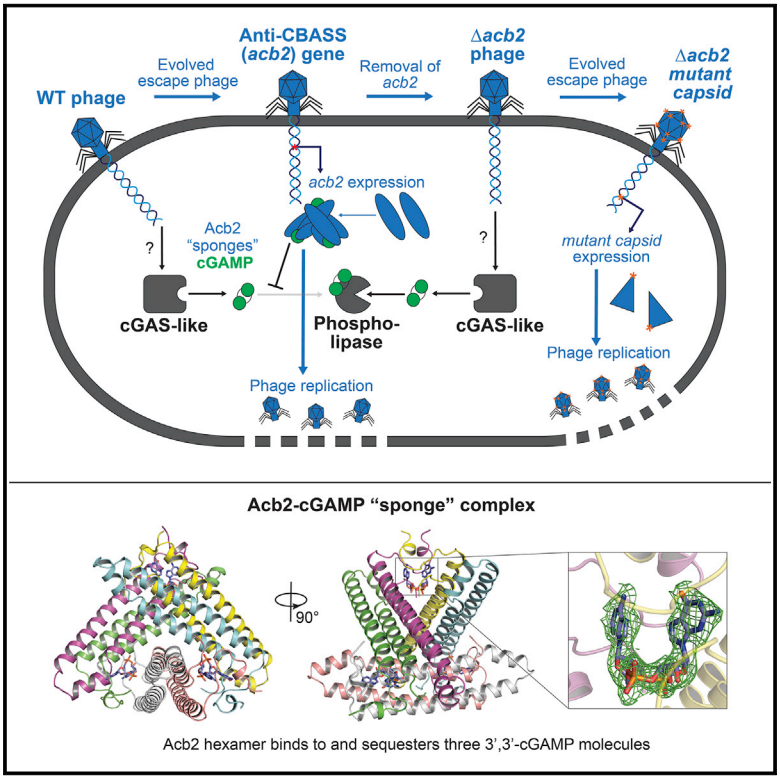

Highlights

- Endogenous *P. aeruginosa* CBASS makes 3′,3′-cGAMP in response to phage infection
- Phages inhibit CBASS via anti-CBASS (Acb2) proteins that sequester 3′,3′-cGAMP
- Acb2 binds to various cyclic dinucleotides: 2′,3′-cGAMP and 3′,3′-cUU/UA/UG/AA
- Diverse phages evade CBASS via mutations in their major capsid gene

Authors

Erin Huiting, Xueli Cao, Jie Ren, ..., James S. Fraser, Yue Feng, Joseph Bondy-Denomy

Correspondence

fengyue@mail.buct.edu.cn (Y.F.), joseph.bondy-denomy@ucsf.edu (J.B.-D.)

In brief

Bacteriophages antagonize cGAS-like bacterial immunity by sequestering immune signaling molecules and acquiring capsid gene mutations.

Huiting et al., 2023, Cell *186*, 1–13
February 16, 2023
https://doi.org/10.1016/j.cell.2022.12.041

CellPress

Cell

CellPress
OPEN ACCESS

Article

Bacteriophages inhibit and evade cGAS-like immune function in bacteria

Erin Huiting,[1,8] Xueli Cao,[2,8] Jie Ren,[3] Januka S. Athukoralage,[1] Zhaorong Luo,[2] Sukrit Silas,[1] Na An,[2] Héloïse Carion,[1] Yu Zhou,[4] James S. Fraser,[5] Yue Feng,[2,*] and Joseph Bondy-Denomy[1,6,7,9,*]

[1]Department of Microbiology and Immunology, University of California, San Francisco, San Francisco, CA 94158, USA
[2]Beijing Advanced Innovation Center for Soft Matter Science and Engineering, Beijing Key Laboratory of Bioprocess, State Key Laboratory of Chemical Resource Engineering, College of Life Science and Technology, Beijing University of Chemical Technology, Beijing 100029, China
[3]State Key Laboratory for Biology of Plant Diseases and Insect Pests, Ministry of Agriculture, Institute of Plant Protection, Chinese Academy of Agricultural Sciences, Beijing 100081, China
[4]National Institute of Biological Sciences, Beijing 102206, China
[5]Department of Bioengineering and Therapeutic Sciences, University of California, San Francisco, San Francisco, CA 94158, USA
[6]Quantitative Biosciences Institute, University of California, San Francisco, San Francisco, CA 94158, USA
[7]Innovative Genomics Institute, Berkeley, CA 94720, USA
[8]These authors contributed equally
[9]Lead contact
*Correspondence: fengyue@mail.buct.edu.cn (Y.F.), joseph.bondy-denomy@ucsf.edu (J.B.-D.)
https://doi.org/10.1016/j.cell.2022.12.041

SUMMARY

A fundamental strategy of eukaryotic antiviral immunity involves the cGAS enzyme, which synthesizes 2′,3′-cGAMP and activates the effector STING. Diverse bacteria contain cGAS-like enzymes that produce cyclic oligonucleotides and induce anti-phage activity, known as CBASS. However, this activity has only been demonstrated through heterologous expression. Whether bacteria harboring CBASS antagonize and co-evolve with phages is unknown. Here, we identified an endogenous cGAS-like enzyme in *Pseudomonas aeruginosa* that generates 3′,3′-cGAMP during phage infection, signals to a phospholipase effector, and limits phage replication. In response, phages express an anti-CBASS protein ("Acb2") that forms a hexamer with three 3′,3′-cGAMP molecules and reduces phospholipase activity. Acb2 also binds to molecules produced by other bacterial cGAS-like enzymes (3',3'-cUU/UA/UG/AA) and mammalian cGAS (2′,3′-cGAMP), suggesting broad inhibition of cGAS-based immunity. Upon Acb2 deletion, CBASS blocks lytic phage replication and lysogenic induction, but rare phages evade CBASS through major capsid gene mutations. Altogether, we demonstrate endogenous CBASS anti-phage function and strategies of CBASS inhibition and evasion.

INTRODUCTION

Sensing specific macromolecules produced or possessed by viruses is a conserved strategy of antiviral immunity across all kingdoms of life.[1,2] In mammalian cells, viral double-stranded DNA (dsDNA) is bound by cyclic GMP-AMP synthase (cGAS) in the cytoplasm.[3,4] The activated cGAS enzyme produces 2′,3′-cyclic GMP-AMP (2′,3′-cGAMP) dinucleotides that bind to the STING (stimulator of interferon genes) effector protein and induces a type I interferon response.[5,6] Recently, thousands of cGAS-like enzymes named cGAS/DncV-like nucleotidyltransferases (CD-NTases) were identified across the entire bacterial domain and then biochemically characterized, revealing at least 8 enzymatic clades and 10 known cyclic oligonucleotides.[7] These enzymes are activated during phage infection through an unknown mechanism and produce cyclic oligonucleotides, like 3′,3′-cGAMP, which activate a downstream effector.[8–12] This strategy of bacterial immunity was coined cyclic-oligonucleotide-based anti-phage signaling system (CBASS).[8] CD-NTases and effectors comprise the core CBASS genes (type I CBASS), and additional "signature" CD-NTase-associated proteins (Caps) have been identified in type II and III CBASS that regulate CD-NTase activity.[10,13–16]

Phage infection introduces nucleic acids and numerous foreign proteins into the bacterial cell. However, molecules that cause a phage to be sensitive or resistant to a given anti-phage immune system are largely unknown. A recent study discovered a family of phage-encoded anti-CBASS phosphodiesterase enzymes (Acb1), which cleaves cyclic oligonucleotides[17] similarly to poxin enzymes encoded by eukaryotic viruses.[18] Investigating the co-evolution of phages and CBASS in a host with endogenous CBASS function will inform how cGAS-based immunity functions in nature and is the main goal of this study.

Please cite this article in press as: Huiting et al., Bacteriophages inhibit and evade cGAS-like immune function in bacteria, Cell (2023), https://doi.org/10.1016/j.cell.2022.12.041

Pseudomonas aeruginosa (*P. aeruginosa*) is a human opportunistic pathogen that encodes a diversity of CBASS operons and is a generalist microbe that survives in many niches. *P. aeruginosa* also has a diverse phage population and is a leading candidate for phage therapy, but our limited understanding of basic anti-phage immunity is a barrier to phage therapeutic development. Here, we identified a *P. aeruginosa* strain that harbors type II-A CBASS (3′,3′-cGAMP producing CD-NTase; CdnA) with a phospholipase (CapV) effector that limits phage replication by ≥10,000-fold. This is a notable finding because it demonstrates that endogenous CBASS anti-phage immunity can function without overexpression. We next identified a widespread phage anti-CBASS protein (Acb2) that forms a hexamer complex with three 3′,3-cGAMP molecules, acting as a "sponge" to reduce the available molecules to activate the phospholipase effector. In addition, Acb2 binds to multiple other cyclic dinucleotides, including 3′,3′-c-di-UMP, 3′,3′-cUA, and 3′,3′-cUG, and is necessary for optimal phage replication in the presence of type I or II CBASS that is predicted to encode the aforementioned cyclic dinucleotides. Phages with *acb2* deleted were unable to replicate in the lytic cycle or during exit from lysogeny in the presence of CBASS. However, mutations in the major capsid gene enabled phages to escape CBASS. This work provides direct evidence of phage inhibition and evasion of CBASS, demonstrating a robust arms race between the two.

RESULTS

Endogenous anti-phage CBASS function in *Pseudomonas aeruginosa*

Previous analyses,[13] coupled with our own bioinformatics, revealed that 252 distinct *P. aeruginosa* strains have >300 CBASS operons (Figures S1A and S1B). These systems span types I–III and use numerous effector proteins and cyclic oligonucleotides.[7] The diverse CBASS types in *P. aeruginosa* suggest that it is important for host fitness and that it may be well suited to study phage-CBASS interactions. To identify naturally functional CBASS immunity in *P. aeruginosa*, CBASS loci were deleted from the genome of four strains possessing representatives of the common CBASS types (types I-A, II-A, II-C, and III-C; Figure S1C), using a CRISPR-Cas3 tool.[19] Notably, these strains also encode numerous other anti-phage immune systems (Figure 1A). Therefore, due to the multitude of immune systems, we screened the CBASS mutants against a diverse panel of ~70 phages, which spanned 23 different genomic families and 4 different morphologies (Myoviridae, Siphoviridae, Podoviridae, and Inoviridae[20]). A single *P. aeruginosa* strain (BWHPSA011; Pa011) was identified with CBASS-dependent anti-phage activity (Figures S1D and S1E).

Deletion of the Pa011 type II-A CBASS operon (ΔCBASS, Figure 1B) resulted in >4 orders of magnitude increase in titer of the dsDNA podophage PaMx41 (Figures 1C and 1D). Phage protection was restored when all four CBASS genes (*capV* [phospholipase effector], *cdnA* [CD-Ntase], *cap2* [E1/E2 ubiquitin-ligase-like domains], and *cap3* [JAB de-ubiquitinating enzyme-like domain]) were complemented on a plasmid (Figure S1G). To determine which genes are necessary for CBASS anti-phage activity, chromosomal mutants known to disrupt catalytic activity[8,15] were generated: $capV^{S48A}$, $cdnA^{D87A/D89A}$, $cap2^{C450A/C453A}$, and $cap3^{E38A}$. Notably, *capV*, *cdnA*, and *cap2* mutations abolished anti-phage activity whereas the *cap3* mutation did not (Figure S1H). Furthermore, using an ELISA, we observed that PaMx41 infection generated low levels of 3′,3′-cGAMP (~8 nM; Figures S2A and S2B), whereas the molecule was nearly undetectable in CdnA mutant strain (~0.5 nM; limit of detection: 0.24 nM). These data demonstrate that Pa011 CBASS-based immunity is naturally active, significantly limits phage replication, and requires CapV, CdnA, and Cap2 enzyme activities for phage targeting.

PaMx41-like phages encode a CBASS antagonist

How CBASS detects and targets phage is currently unknown. Therefore, to identify phage genes required for successful CBASS activity, we isolated PaMx41 mutants that resist Pa011 CBASS-based immunity. With a frequency of 3.7×10^{-5} (Figure 1D), 10 independent PaMx41 CBASS "escape" phages were isolated that replicate well on Pa011 wild type (WT). Whole-genome sequencing revealed one mutation in all CBASS escape phages: a no-stop extension mutation (X37Q) in *orf24* (Figure 1E). X37Q lengthens gp24 from a 37 amino acid (aa) protein to 94 aa. Interestingly, the naturally CBASS-resistant phages, PaMx33, PaMx35, and PaMx43, share >96% nucleotide identity across the genome and naturally encode the 94 aa version with >98% aa identity.

To determine whether the short gp24 activates CBASS or the long gp24 antagonizes it, the PaMx41 gp24 variants were overexpressed in Pa011 WT and ΔCBASS cells, and then plaque assays were performed. In the presence of CBASS, the long gp24 increased the titer of the PaMx41 WT phage by ≥4 orders of magnitude, whereas the truncated gp24 versions had no effect (Figure 1F). By contrast, the PaMx41 escaper phage and PaMx33, PaMx35, and PaMx43 phages exhibited high titer on all strains (Figure S2C), demonstrating that the short gene is not a dominant CBASS activator. We next deleted *orf24* from all of the resistant PaMx41-like phages, using a Cas13a selection tool, because these phages were surprisingly resistant to all tested DNA-targeting CRISPR-Cas systems.[21] In Pa011 WT cells, the titer of the *Δorf24* phages was reduced 2–4 orders of magnitude; however, expression of the long gp24 in *trans* rescued the phages (Figures 2A, 2B, and S2D). Taken together, these results indicate that the long gp24, or Acb2 (anti-CBASS 2; PaMx33 Genbank: ANA48877) hereafter, inhibits Pa011 CBASS immunity and is necessary for phage replication in the presence of CBASS.

Acb2 has conserved function in a broadly distributed temperate phage family

Homology searches with Acb2 revealed that it is encoded in a striking number of tailed phages, including those infecting *Pseudomonas*, *Vibrio*, *Acinetobacter*, *Salmonella*, *Serratia*, *Erwinia*, and *Escherichia* sp. (T2 and T4 phages; gene *vs.4*), among others (Figure S3A). We observed no other examples of the truncated Acb2 variant encoded in PaMx41 WT phage. A multi-sequence alignment with diverse homologs revealed highly conserved N and C termini with a middle region of varied length and sequence (Figure S3B), but no molecular function could be predicted.

Please cite this article in press as: Huiting et al., Bacteriophages inhibit and evade cGAS-like immune function in bacteria, Cell (2023), https://doi.org/10.1016/j.cell.2022.12.041

CellPress
OPEN ACCESS

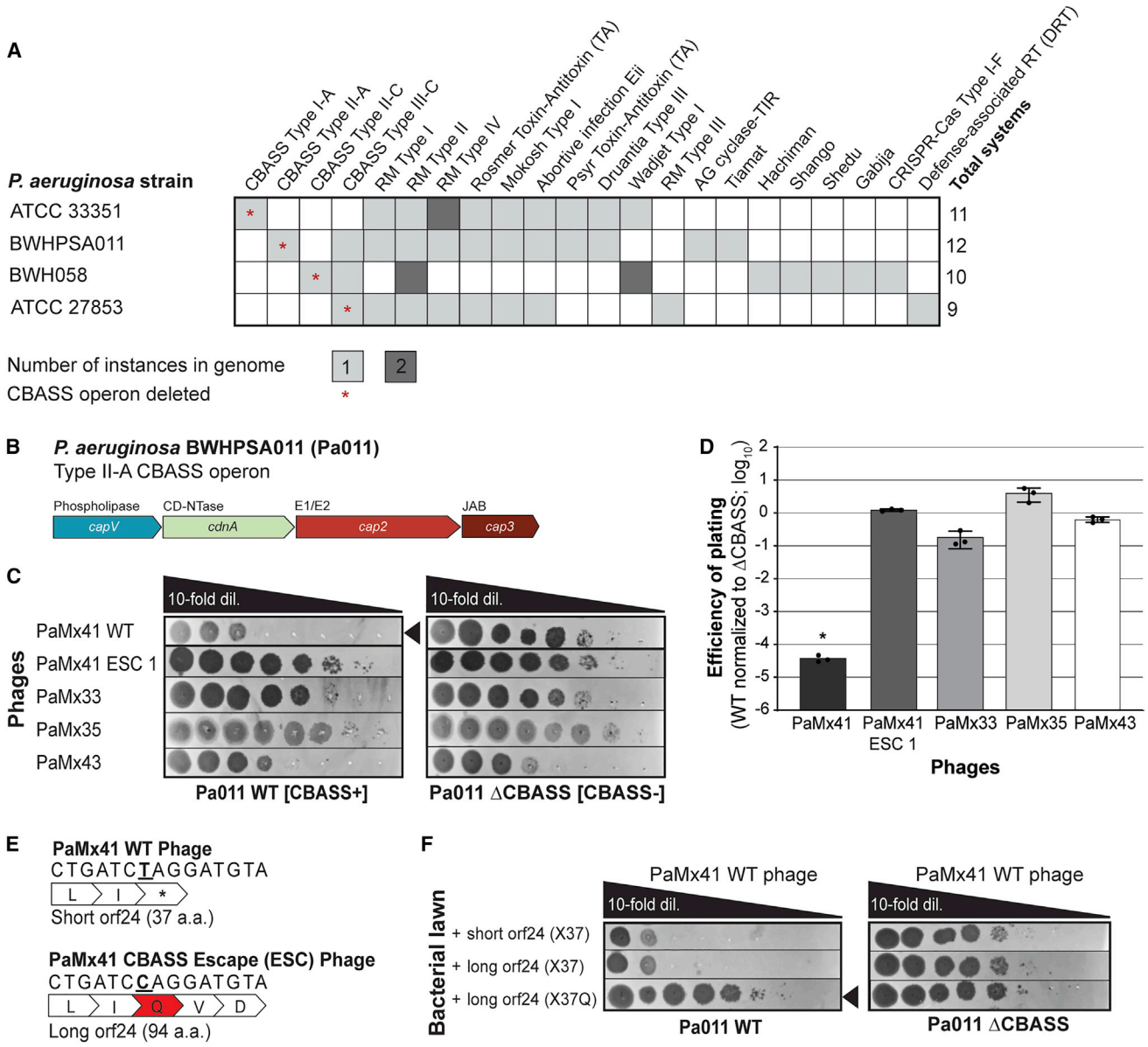

Figure 1. *P. aeruginosa* BWHPSA011 (Pa011) CBASS-based immunity protects against PaMx41 infection

(A) The presence of different anti-phage immune systems in *P. aeruginosa* strains that were used in this study. Some systems are present in the genome twice as indicated by the darker shade of gray and number (2). An asterisk (*) indicates the CBASS operon was effectively deleted from the bacterial genome.

(B) Pa011 CBASS operon.

(C) Plaque assays with PaMx41-like phages and an evolved PaMx41 CBASS Escaper (ESC) phage spotted in 10-fold serial dilutions on a lawn of Pa011 WT [CBASS+] or ΔCBASS [CBASS−]; clearings represent phage replication. Black arrowhead highlights the reduction in PaMx41 WT phage titer. See also Figure S1.

(D) Efficiency of plating was quantified as plaque-forming units (PFUs) per mL on Pa011 WT divided by PFU/mL on the ΔCBASS (n = 3). Data are mean ± SD. Non-parametric ANOVA test yielded a p value of <0.0001.

(E) Schematic of PaMx41 WT and CBASS escape phage genomes with the no-stop extension mutation. The bold underline indicates mutation of thymine (T) to cytosine (C), resulting in a stop codon (TAG, *) to glutamine (CAG, Q) substitution (in red).

(F) Plaque assays with PaMx41 WT phage on a lawn of Pa011 WT or ΔCBASS overexpressing the indicated *orf24* variants. See also Figure S2.

Furthermore, *acb2* is commonly encoded by *P. aeruginosa* B3-like temperate phages (e.g., JBD67), which are unrelated to the PaMx41-like lytic phages. Since JBD67 phage does not replicate on the Pa011 strains, we integrated the type II-A CBASS operon with its native promoter into the chromosome of a *P. aeruginosa* strain (POA1) that is sensitive to this phage and naturally lacks CBASS. This engineered strain (Pa^{CBASS}) was active and reduced PaMx41 WT phage titer by 3–4 orders of magnitude (Figures S1D and S1F). By contrast, JBD67 exhibited resistance to the Pa^{CBASS} strain, while a related phage that naturally lacks

Please cite this article in press as: Huiting et al., Bacteriophages inhibit and evade cGAS-like immune function in bacteria, Cell (2023), https://doi.org/10.1016/j.cell.2022.12.041

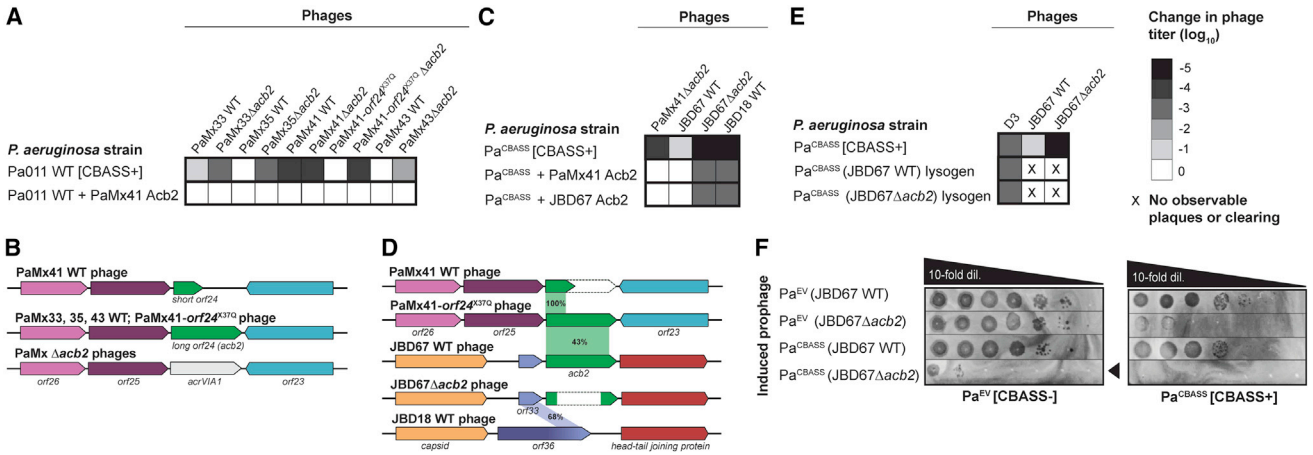

Figure 2. Phage-encoded *acb2* is necessary for replication in the presence of CBASS

(A, C, and E) Heatmaps representing the order of magnitude change in phage titer, where phage titer is quantified by comparing the number of spots (with plaques, or clearing if plaques were not visible) on the CBASS+ strain divided by the CBASS− strain. Plaque assays used for these quantifications can been seen in Figure S2 (n = 3).

(B and D) Comparison of the *acb2* locus across phage genomes. PaMx41-like Δ*acb2* phages have the *acb2* gene substituted with the type VI-A anti-CRISPR gene (*acrVIA1*) as part of the knockout procedure, and JBD67Δ*acb2* phages have the *acb2* gene removed from its genome. Genes with known protein functions are indicated with names, and genes with hypothetical proteins are indicated with "*orf*." Acb2 percent amino acid identity is shown in (D).

(F) Plaque assays assessing the titer-induced prophages spotted on a lawn of Pa^{EV} or Pa^{CBASS}. Black arrowhead highlights reduction in JBD67Δ*acb2* phage titer. See also Figure S2.

the *acb2* gene, JBD18, was robustly inhibited (Figures 2C, 2D, and S2E). Deletion of *acb2* from JBD67, using a helicase attenuated Cascade-Cas3 system (see STAR Methods), sensitized it to CBASS immunity (Figures 2C, 2D, and S2E). The titer of JBD67Δ*acb2* and JBD18 phages were reduced by ≥5 orders of magnitude in the presence of CBASS. Expression of *acb2* derived from either JBD67 or PaMx41-*orf24*^{X37Q} on a plasmid fully restored the titer of the PaMx41Δ*acb2* phage, and only partially restored the titer of the JBD67Δ*acb2* and JBD18 phages (Figures 2C and S2E). We hypothesize that JBD67 and JBD18 more strongly activate CBASS, and consequently, Acb2 expression in *trans* becomes partially overwhelmed. Together, these results collectively demonstrate that *acb2* retains its anti-CBASS function across distinct phage families.

Given that JBD67 is a temperate phage, we investigated whether *acb2* is active during lysogeny as a prophage and therefore inhibits a co-encoded CBASS system. Lysogens were constructed with JBD67 in the Pa^{CBASS} strain, where CBASS targets the super-infecting phage D3. JBD67 and D3 are from hetero-immune groups, so there is no super-infection exclusion between these phages. Interestingly, the degree to which CBASS targets D3 was not impacted by the presence of *acb2* in the JBD67 prophage (Figures 2E and S2F). This suggests that *acb2* is not expressed during lysogeny and allows for functional CBASS immunity despite a prophage-encoded inhibitor. However, upon exit from lysogeny, CBASS significantly blocks JBD67Δ*acb2* prophage induction, reducing the induced titer by ~5 orders of magnitude, whereas JBD67 WT prophage induction was unaffected (Figure 2F). These collective findings demonstrate that *acb2* is active during lysogenic induction, but not lysogenic maintenance, and importantly show that CBASS can dramatically limit prophage induction.

Acb2 sequesters 3′,3′-cGAMP to inhibit CBASS

To determine the mechanism of Acb2, we purified Acb2 from the naturally CBASS-resistant PaMx33 phage and each CBASS protein to test direct CBASS antagonism. First, we tested binding and found that Acb2 did not bind to purified CapV, CdnA, Cap2, nor the CdnA-Cap2 complex, which were purified as described previously (Figures S4A–S4D; Ledvina et al.[15]). Next, we reconstituted CapV phospholipase activity *in vitro* and confirmed that it is only activated by 3′,3′-cGAMP in a concentration-dependent manner but not by 2′,3′-cGAMP, c-di-AMP, or c-di-GMP (Figure 3A). When Acb2 was preincubated with 3′,3′-cGAMP, CapV activity was abrogated (Figure 3A), suggesting that Acb2 may directly bind to the 3′,3′-cGAMP molecule. A native gel assay showed a significant shift of the purified Acb2 protein upon adding 3′,3′-cGAMP (Figure 3B). Isothermal calorimetry (ITC) experiments further verified that Acb2 directly binds to 3′,3′-cGAMP with a K_D of ~87 nM (Figures 3C and S4E). Together, these data suggest that Acb2 binding of 3′,3′-cGAMP antagonizes CBASS by reducing available signaling molecules.

Recent studies have reported that eukaryotic[18] and prokaryotic[17,22] viruses express proteins that directly degrade cyclic oligonucleotides. Therefore, to determine whether Acb2 is an enzyme that cleaves 3′,3′-cGAMP molecules, we performed the CapV phospholipase activity assay using a series of Acb2 concentrations and Acb2-3′,3′-cGAMP incubation times. Inhibition of CapV activity was concentration-dependent, but not time-dependent (Figure 3D), suggesting that Acb2 is a protein that sponges and sequesters 3′,3′-cGAMP rather than degrade it. High-performance liquid chromatography (HPLC) clearly showed that incubation of Acb2 depletes detectable 3′,3′-cGAMP, and following proteolysis of Acb2, the molecule is released back into the buffer (Figure 3E). Filtration of the

Please cite this article in press as: Huiting et al., Bacteriophages inhibit and evade cGAS-like immune function in bacteria, Cell (2023), https://doi.org/10.1016/j.cell.2022.12.041

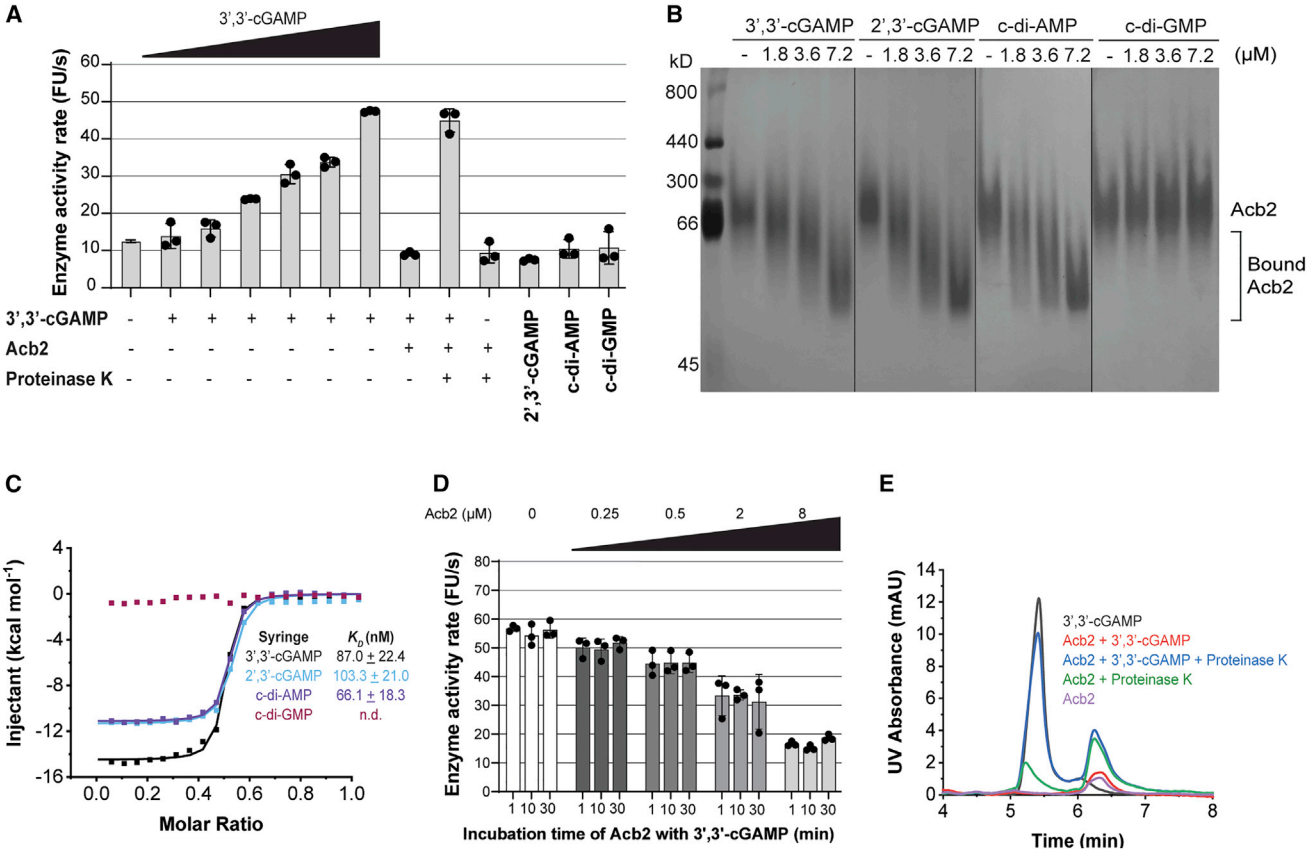

Figure 3. Acb2 antagonizes CBASS activity by sequestering the 3′,3′-cGAMP signaling molecule

(A) CapV enzyme activity in the presence of the indicated cyclic dinucleotides and resorufin butyrate, which is a phospholipase substrate that emits fluorescence when hydrolyzed. The enzyme activity rate was measured by the accumulation rate of fluorescence units (FUs) per second. The concentration of 3′,3′-cGAMP ranged from 0.025 to 0.8 μM (0.025, 0.05, 0.1, 0.2, 0.4, and 0.8 μM), and the other cyclic dinucleotides were added at 0.8 μM. To test the effects of Acb2 to bind and release 3′,3′-cGAMP, Acb2 (32 μM) was incubated with 3′,3′-cGAMP (0.8 μM) for 10 min and then proteinase K (0.065 mg/mL) was added to extract the nucleotides from the Acb2 protein. Filtered nucleotide products were used for the CapV activity assay. Data are mean ± SD (n = 3).

(B) Native PAGE showed the binding of Acb2 to cyclic dinucleotides.

(C) Isothermal titration calorimetry (ITC) assays to test binding of cyclic dinucleotides to Acb2. Representative binding curves and binding affinities are shown. The K_D values are mean ± SD (n = 3). Raw data for these curves are shown in Figure S4.

(D) CapV activity assay to test the effects of Acb2 on 3′,3′-cGAMP. The concentration of 3′,3′-cGAMP was 0.8 μM, and Acb2 ranged from 0.25 to 8 μM (0.25, 0.5, 2, and 8 μM). The 3′,3′-cGAMP was preincubated with Acb2 for 1, 10, and 30 min, respectively. Data are mean ± SD (n = 3).

(E) The ability of Acb2 to bind and release 3′,3′-cGAMP when treated with proteinase K was analyzed by HPLC. 3′,3′-cGAMP standard was used as a control. The remaining 3′,3′-cGAMP after incubation with Acb2 was tested.

unbound 3′,3′-cGAMP enabled CapV to regain its enzymatic activity, demonstrating that the molecule is still active (Figure 3A). Consistent with these results, overexpression of Acb2 in phage-infected Pa011 WT cells reduced detectable 3′,3′-cGAMP levels, but following phenol-chloroform/chloroform nucleotide extraction, the molecule was released and levels increased ~4-fold (Figures S2A and S2B). Altogether, these results demonstrate that Acb2 antagonizes type II-A CBASS immunity via binding and sequestering the 3′3′-cGAMP dinucleotide, which prevents phospholipase effector activation.

Crystal structure of Acb2 and its complex with 3′,3′-cGAMP

To further understand how Acb2 interacts with 3′,3′-cGAMP, we determined the crystal structures of apo Acb2 and its complex with the signaling molecule (Table 1). Interestingly, Acb2 folds as a homo-hexamer in its apo (Figure 4A) and 3′,3′-cGAMP bound form (Figure 4B). Analytical ultracentrifugation (AUC) assay also indicated that Acb2 is a hexamer in its apo and 3′,3′-cGAMP-bound forms in solution (Figures S5A–S5E). Each protomer mainly interacts with two adjacent protomers (Figure S5B), allowing the six protomers to interlock into a compact assembly. An Acb2 protomer consists of one short N-terminal helix and two long anti-parallel helices, with a kink in the long helix at the C terminus (Figure S5C). The ligand-bound structure showed that one Acb2 hexamer binds three 3′,3′-cGAMP molecules (Figure 4B). Each cGAMP-binding pocket is formed by two Acb2 protomers that interact in a head-to-head manner and is mainly composed of N- and C-terminal helices/loops from each protomer (Figure S5D). This is consistent with the Acb2

Please cite this article in press as: Huiting et al., Bacteriophages inhibit and evade cGAS-like immune function in bacteria, Cell (2023), https://doi.org/10.1016/j.cell.2022.12.041

Table 1. Data collection and refinement statistics

	Acb2	Acb2-3',3'-cGAMP	Acb2-c-di-AMP
PDB code	8H2X	8H2J	8H39
Data collection			
Space group	P321	P321	P321
Cell dimensions			
a, *b*, *c* (Å)	101.9, 101.9, 101.7	103.5, 103.5, 101.6	104.1, 104.1, 102.0
(°)	90.00, 90.00, 120.00	90.00, 90.00, 120.00	90.00, 90.00, 120.00
Resolution (Å)	50–2.69 (2.79–2.69)[a]	12.87–2.40 (2.49–2.40)	67.58–2.01 (2.11–2.01)
R_{sym} or R_{merge} (%)	16.9 (66.6)	8.3 (41.6)	9.2 (122.8)
$I/\sigma(I)$	16.6 (3.0)	31.8 (5.7)	21.0 (2.8)
Completeness (%)	99.9 (100.0)	99.2 (100.0)	100.0 (100.0)
Redundancy	14.1 (10.2)	22.3 (21.9)	20.0 (20.4)
Refinement			
Resolution (Å)	33.37–2.69 (2.79–2.69)	12.87–2.40 (2.49–2.40)	67.58–2.01 (2.08–2.01)
Unique reflection	17,084 (1,624)	24,843 (2,448)	43,247 (6,272)
R_{work} / R_{free}[b]	0.250/0.269	0.244/0.279	0.209/0.233
No. atoms	4,449	4,704	4,859
Protein	4,302	4,396	4,365
Ligand/ion	62	180	208
Water	85	128	286
B factors	52.64	50.22	44.81
Protein	53.23	50.70	45.12
Ligand/ion	38.93	44.72	38.41
Water	32.44	41.57	44.80
RMS deviations			
Bond lengths (Å)	0.010	0.005	0.004
Bond angles (°)	1.58	1.00	0.60
Ramachandran plot (%)			
Favored	97.90	97.01	98.31
Allowed	2.10	2.99	1.69
Outliers	0.00	0.00	0.00

[a]Values in parentheses are for highest-resolution shell.
[b]For each structure, one crystal was used.

multiple sequence alignment, which revealed highly conserved N and C termini (Figure S3B). Searches using the distance-matrix alignment (Dali) server did not return entries with the same protein fold as Acb2,[23] indicating that Acb2 adopts an overall novel cyclic dinucleotide-binding fold. In support of these findings, a recent preprint[16] demonstrated that the Acb2 homolog from *E. coli* phage T4 (gene *vs.4*) tightly binds to 3′,3′-cGAMP (K_D of ~30 nM) and adopts a hexameric structure similar to the one reported here.

Acb2 binding of a cyclic dinucleotide ligand only causes a slight movement of the loop linking α1 and α2 (named loop L12) toward the ligand (Figure 4D), but several other residues display rotations and movements upon ligand binding. Among them, the most dramatic movement happens in Y11 from both protomers, which rotates and forms π-π interactions with the purine bases of cGAMP, as well as hydrogen bonds with the phosphate group of cGAMP (Figure 4E). In addition, K26 in α2 of both protomers forms a salt bridge with the phosphate group of the cGAMP, possibly stabilizing the molecule together with Y11 (Figure 4F). Additionally, cGAMP is stabilized through hydrophobic interactions by several residues from both protomers, such as L14, M22, M81, I84, and P90 (Figure 4F). Consistent with these analyses, Acb2 Y11A and K26A mutants were inactive in plaque assays (Figure 4I), and the Acb2 K26A mutant expressed in the Pa011 WT strain lost its ability to sequester 3′,3′-cGAMP *in vivo* (Figures S2A and S2B). Furthermore, Acb2 Y11A and K26A mutants abolished Acb2 binding of 3′,3′-cGAMP *in vitro* (Figures 4G and S4I–S4K) and abrogated its ability to reduce CapV activity (Figure 4H). These data collectively show that Acb2 proteins form a complex with cyclic dinucleotides and subsequently reduce downstream CBASS activation.

Acb2 sequesters variety of cyclic dinucleotides

The binding mode of 3′,3′-cGAMP within Acb2 implied that other cyclic dinucleotides could also be sequestered by this protein. Indeed, native gels and ITC experiments demonstrated that

Please cite this article in press as: Huiting et al., Bacteriophages inhibit and evade cGAS-like immune function in bacteria, Cell (2023), https://doi.org/10.1016/j.cell.2022.12.041

CellPress
OPEN ACCESS

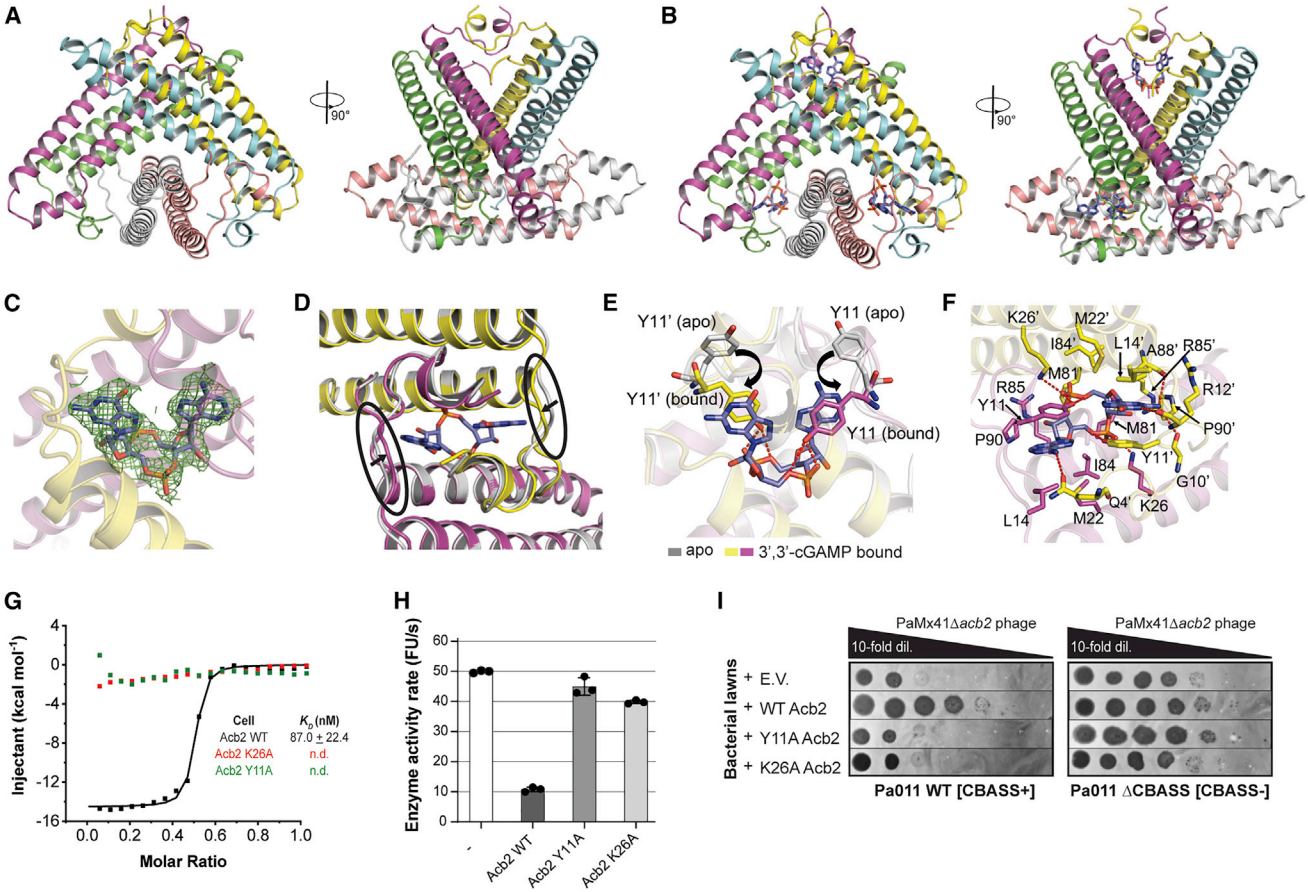

Figure 4. Structure of Acb2 reveals hexamer bound to three molecules of 3′,3′-cGAMP

(A) Overall structure of the Acb2 hexamer. Two views are shown.

(B) Overall structure of the Acb2 hexamer bound to three molecules of 3′,3′-cGAMP. 3′,3′-cGAMP molecules are colored in slate.

(C) 2Fo-Fc electron density of 3′,3′-cGAMP in the binding pocket contoured at 1 σ.

(D) Structural comparison between an Acb2 dimer in its apo (colored in gray) and 3′,3′-cGAMP-bound form (colored in yellow and light magenta). The loops that move upon 3′,3′-cGAMP binding are marked with black circles.

(E) Structural alignment between apo and 3′,3′-cGAMP-bound Acb2, which are colored as in (B). Y11 from the two structures are highlighted as sticks. Red dashed lines represent polar interactions.

(F) Binding between Acb2 or Acb2 mutants and 3′,3′-cGAMP. Red dashed lines represent polar interactions.

(G) ITC assays to test the binding of 3′,3′-cGAMP to Acb2 mutants. Representative binding curves and binding affinities are shown. The K_D values are mean ± SD (n = 3). Raw data for these curves are shown in Figure S4.

(H) CapV activity assay to test the effects of Acb2 mutations. The concentration of 3′,3′-cGAMP was 0.8 μM and of Acb2 or its mutants was 32 μM. The 3′,3′-cGAMP was preincubated with Acb2 or its mutants for 10 min. Bar graph represents average of three technical replicates. Data are mean ± SD (n = 3).

(I) Plaque assays on a lawn of Pa011 WT or ΔCBASS overexpressing empty vector (E.V.) or the indicated PaMx41 Acb2 mutants; clearings represent phage replication.

Acb2 also binds to 2′,3′-cGAMP and c-di-AMP with high affinity (K_D of ~103 and 66 nM, respectively), but not c-di-GMP (Figures 3B, 3C, S4F, and S4G). HPLC assays confirmed that Acb2 could sequester c-di-AMP and 2′,3′-cGAMP, and showed a very weak sequestering effect on c-di-GMP (Figures S5F–S5H). The Acb2-c-di-AMP structure was also solved (Table 1), and c-di-AMP showed a similar binding mode as 3′,3′-cGAMP (Figures S5I–S5K). Additional native gels and ITC experiments showed that Acb2 can bind to 3′,3′-c-di-UMP (cUU) and 3′,3′-c-UMP-AMP (cUA) with high affinity (K_D of ~99 and 97 nM, respectively), and it binds to 3′,3′-c-UMP-GMP (cUG) with lower affinity (K_D of ~524 nM) (Figures S6A–S6E).

Next, we tested whether phages expressing *acb2* could inhibit CBASS subtypes *in vivo* that harbor a CdnE cyclase, which are predicted to generate cUU, cUA, and/or cUG (A. Whiteley, personal communication).[7] In our strain collection, we identified that *P. aeruginosa* strains ATCC 33351 and JD332 encode type I-A and type I-B CBASS operons, respectively, with a CdnE cyclase (Figures 1A and S6F). When these systems were cloned and expressed in a *P. aeruginosa* strain (PAO1 WT) that naturally lacks CBASS, the titer of phages lacking *acb2* was reduced 1–3 orders of magnitude—most notably by JD332 type I-B CBASS—and the isogenic phages containing *acb2* remained resistant to CBASS (Figure S6G). Together, these

Please cite this article in press as: Huiting et al., Bacteriophages inhibit and evade cGAS-like immune function in bacteria, Cell (2023), https://doi.org/10.1016/j.cell.2022.12.041

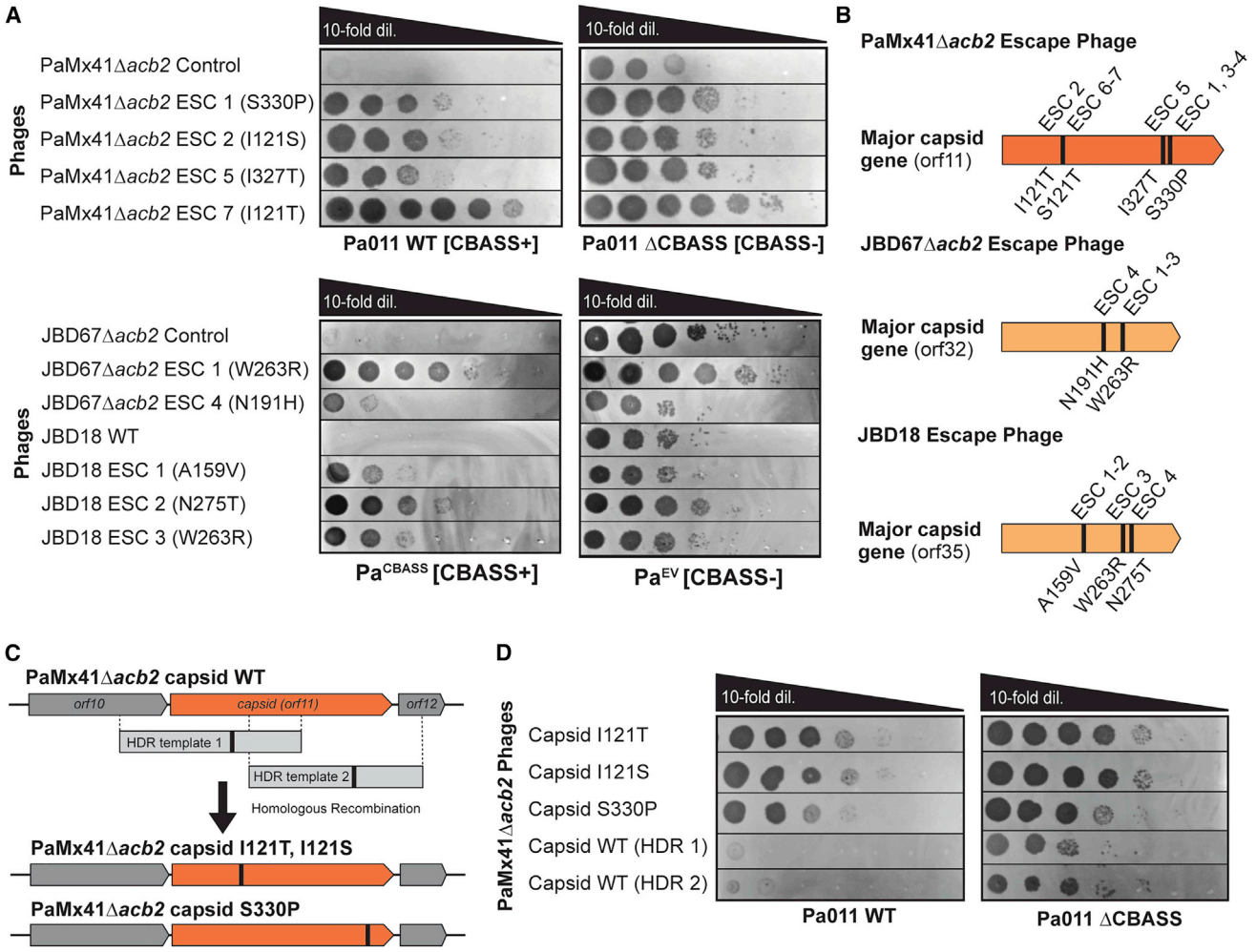

Figure 5. CBASS escape phages have mutations in the major capsid gene

(A) Plaque assays were performed with the indicated control/WT and escape phages spotted in 10-fold serial dilutions on lawns of bacteria expressing CBASS+ (left) or lacking CBASS− (right); clearings represent phage replication.

(B) Schematic of major capsid genes with corresponding missense mutations and associated CBASS escape (ESC) phages.

(C) Schematic of *in vivo* homologous recombination of parental phages with homology-directed repair (HDR) template 1 (encoding I121S or I121T capsid mutations) or template 2 (S330P capsid mutation) and resultant engineered/recombinant phages.

(D) Plaque assays with recombinant phages possessing major capsid mutations, or WT capsid controls, spotted on lawns of Pa011 WT or ΔCBASS.

in vitro and *in vivo* results suggest that Acb2 can broadly inhibit CBASS types that utilize cyclic dinucleotides with uracil and adenine bases.

Phages escape CBASS via mutations in the capsid gene

The function and mechanism of *acb2* demonstrates that CBASS places strong evolutionary pressure on phage. Therefore, we sought to determine whether any alternative mechanisms to evade CBASS exist. We again attempted to identify mutant escape phages, but this time, we used phage lacking *acb2* (PaMx41Δ*acb2*). Phages were first exposed directly to CBASS by plating on Pa011 WT, which yielded no escape plaques. However, the invisible phage population on the plate was collected, amplified in the Pa011 ΔCBASS strain, and ultimately escape phages were isolated under CBASS selection (Figure 5A). Whole-genome sequencing revealed that all seven escape phages had one of four different missense point mutations in the major capsid gene (*orf11*, NCBI: YP_010088887.1; Figure 5B; Table S1). To confirm the causality of the capsid mutations for CBASS escape, we used plasmid-based recombination to introduce *de novo* mutations I121A, I121T, and S330P into a naive PaMx41Δ*acb2* phage and confirmed that these mutations induced CBASS escape (Figures 5C and 5D). To test whether the major capsid is sufficient to trigger CBASS, the PaMx41 WT or mutant major capsid gene with its native promoter was cloned and expressed in Pa011 WT and ΔCBASS cells. In the presence of the WT major capsid, we did not observe any CBASS-dependent cellular toxicity, indicating that capsid monomer is not sufficient to activate CBASS. We also did not observe CBASS-dependent targeting of resistant phage

(Figure S7A). Likewise, expression of the mutant major capsid gene did not induce escape of CBASS-sensitive phage (Figure S7B). We anticipate that the plasmid-encoded major capsid gene does not express well enough to sufficiently displace the phage-expressed major capsid gene in a manner that impacts the CBASS phenotype.

CBASS escape phages were also isolated from JBD67Δ*acb2* and JBD18 phages on the Pa^{CBASS} strain (Figure 5A). Strikingly, whole-genome sequencing revealed missense point mutations in the genes encoding their major capsid proteins (*orf32* in JBD67 [NCBI: YP_009625956] and *orf35* in JBD18 [NCBI: AFR52188]; Figure 5B; Table S1). The PaMx41 major capsid protein shares no significant amino acid identity with the JBD67 and JBD18 major capsid proteins, yet the mutations all converge on the same protein. When modeling the location of the mutations on the predicted major capsid monomer structures, we did not observe overlap between the distinct phages (Figure S7C). However, modeling of the predicted major capsid hexamer structures indicated that the mutations lie on the protein-protein interface within or between hexamers (Figures S7D and S7E), suggesting that a higher ordered capsid structure or process may be implicated in CBASS immunity. Interestingly, some of the observed capsid mutant genotypes (i.e., I121S/T from PaMx41, N191H from JBD67, and N275D from JBD18) are common natural alleles in the capsids of other phages. Follow-up studies are needed to determine the mechanistic connection between the major capsid protein and CBASS.

DISCUSSION

The discovery and characterization of CBASS marked an exciting connection between prokaryotic and eukaryotic immunity.[7,8] However, many questions remain in this nascent field regarding phage-host evolution, as well as CBASS regulation and activation mechanisms, that can be best addressed through utilization of endogenous CBASS model systems. We found that the *P. aeruginosa* BWHPSA011 (Pa011) strain harbors a cGAS-like enzyme (CdnA) that produces 3′,3′-cGAMP dinucleotides in response to PaMx41 phage infection, which activates the phospholipase (CapV) effector. Phages related to PaMx41 (or an escape mutant derived from PaMx41) produce an anti-CBASS protein (Acb2) that is expressed as a middle gene in the phage replication cycle[24] and sequesters 3′,3′-cGAMP. Acb2 likely accumulates prior to the production of the dinucleotide given that previous work demonstrated 3′,3′-cGAMP levels increase later in the *E. coli* phage P1 replication cycle.[8] Furthermore, when studying the temperate phage JBD67 with its *acb2* gene removed, we found that CBASS limits prophage induction *and* lytic phage replication, which had not been previously noted.

The cyclic dinucleotide sponge protein discovered in this study, Acb2, joins an expanding repertoire of phage-encoded antagonists that directly act on signaling molecules involved in bacterial anti-phage immunity. Previous examples include the anti-CRISPR (AcrIII1) protein that cleaves c-A_4 molecules[22] and the anti-Pycsar (Apyc1) protein that cleaves a spectrum of cyclic nucleotides.[17] In parallel, a Thoeris anti-defense (Tad1) protein was found to specifically bind to and sequester gcADPR molecules.[25] Additionally, the anti-CBASS gene identified (Acb1) is another class of phage enzymes, similar to Apyc1, that harbors a phosphodiesterase fold that specifically binds and cleaves cyclic nucleotides.[17] This is a common inhibitory mechanism of the eukaryotic cGAS-STING signaling system and is utilized by poxviruses[18] and a host pyrophosphatase/phosphodiesterase protein,[26] which enzymatically cleaves and depletes 2′,3′-cGAMP. By contrast, Acb2 binds to and sequesters bacterial 3′,3′-cGAMP, c-di-AMP, 3′,3′-c-di-UMP, 3′,3′-cUA, 3′,3′-cUG, and human 2′,3′-cGAMP. The structure and mechanism of Acb2 were independently confirmed with a homolog from *E. coli* phage T4 in a recent preprint.[16] Despite the numerous different mechanisms employed by viruses to inhibit the eukaryotic cGAS-STING signaling system,[27] the cGAMP sponge mechanism is an entirely new inhibitory strategy.

The identification of capsid mutants that escape CBASS mirrors the recently identified major capsid mutations in *E. coli* phage T5, which enables escape from pyrimidine cyclase system for anti-phage resistance (Pycsar).[28] This study also noted that expression of the T5 WT major capsid protein alone did not induce Pycsar-mediated toxicity, which we similarly observed, nor was direct binding observed between the T5 major capsid protein and any of the Pycsar proteins,[28] suggesting a more complex or indirect activation mechanism. However, abortive immune systems can be activated through direct binding to a capsid monomer, such as the $CapRel^{SJ46}$ toxin-antitoxin system[29] and the Lit protease.[30] These mechanistically diverse systems all converge on the phage capsid protein, which is one of many phage structural proteins mutated to evade targeting of anti-phage bacterial immune systems.[31] Additionally, binding to other phage structural proteins directly activate antiviral STAND NTPases (Avs)[32] and defense-associated sirtuins (DSRs) systems.[33] The major capsid gene mutations identified in our study are enriched at the capsid protein interface, suggesting that a higher ordered capsid structure or process, rather than a capsid monomer, may be implicated in CBASS immunity. However, the mechanism behind the mutant phage capsid that enables CBASS evasion is unknown and remains an area of future investigation. Altogether, we present direct evidence of CBASS as an anti-phage bacterial immune system, uncover distinct paths taken by phage to inhibit or evade immunity, and expand our understanding of viral evasion strategies of cGAS-based immunity.

Limitations of the study

Here, we report the establishment of a native CBASS model system and used it to identify phage mutants that inhibit or evade CBASS. We were unable to establish additional native CBASS model systems because we could not identify phages targeted in a CBASS-dependent manner, which is likely because *P. aeruginosa* harbors several diverse anti-phage systems, and a single strain alone can encode 1–17 (known) systems.[34,35] Furthermore, we describe a cyclic dinucleotide sponge (Acb2) as a mechanism to inhibit multiple cGAS-based immune systems. However, we have not comprehensively sampled the array of cyclic oligonucleotides that this protein family may bind to, which should be completed to further define the selectivity of the new Acb2 protein fold. An additional limitation of our study is that *in vivo* 3′,3′-cGAMP measurements reveal a low

intracellular concentration (<10 nM), which is likely due to lower expression of CBASS genes compared with previous studies. It is also possible that uninfected cells or asynchronous infection leads to lower 3′,3′-cGAMP levels, and given that our measurement represents an average of the entire cell population, the total 3′,3′-cGAMP levels are lower. Lastly, our study identified that phage capsid mutants evade CBASS targeting. Despite this, it is unknown whether the phage capsid evades the activation of the cyclase (CdnA), regulation of the cyclase (via Cap2 or Cap3), targeting of the CapV effector, or evades another stage of CBASS that has yet to be studied.

STAR★METHODS

Detailed methods are provided in the online version of this paper and include the following:

- KEY RESOURCES TABLE
- RESOURCE AVAILABILITY
  - Lead contact
  - Materials availability
  - Data and code availability
- EXPERIMENTAL MODEL AND SUBJECT DETAILS
  - Bacterial strains and phages
- METHOD DETAILS
  - Identification of CBASS operons
  - Identification of anti-phage immune systems
  - Episomal gene expression
  - Site-directed mutagenesis
  - Chromosomal CBASS integration
  - Chromosomal mutants of *P. aeruginosa* BWHPSA011
  - Phage growth
  - Plaque assays
  - Lysogen construction with JDB67 phage
  - Isolation of CBASS phage escapers
  - Whole genome sequencing (WGS) and analysis
  - CRISPR-Cas13a phage gene editing
  - Homologous recombination-mediated mutation of phage gene
  - Helicase attenuated Cas3 removal of phage genes
  - Intracellular 3',3'-cGAMP measurements
  - Phylogenetic analysis
  - Computational modeling of phage capsid
  - Protein expression and purification
  - Crystallization, data collection and structural determination
  - Isothermal titration calorimetry binding assay
  - Fluorogenic biochemical assay for CapV activity
  - Gel filtration assay
  - Analytical ultracentrifugation
  - Native-PAGE assay
  - High-performance liquid chromatography (HPLC)
- QUANTIFICATION AND STATISTICAL ANALYSIS

SUPPLEMENTAL INFORMATION

Supplemental information can be found online at https://doi.org/10.1016/j.cell.2022.12.041.

ACKNOWLEDGMENTS

We thank current and past members of the Bondy-Denomy Lab for thoughtful discussions, including Drs. Bálint Csörgo, Lina León, and Yuping Li for their technical expertise and knowledge of bacterial and molecular genetics; Dr. Jingwen Guan for assistance with Cas13a engineering of PaMx41-like phages; Drs. Shweta Karambelkar and Lina León for the CRISPR-Cas3 helicase attenuated technology to delete JBD67 *acb2*; and Matt Johnson for bioinformatic comparison of phage genomes. We thank Dr. Deborah Hung at the Broad Institute of MIT and Harvard for the *Pseudomonas aeruginosa* strains BWHPSA011 and BWH058. We thank Dr. Jeremy R. Dettman at the University of Ottawa for the sample of *P. aeruginosa* strain JD332. We thank Dr. Gabriel Guarneros Peña at Centro de Investigacion y de Estudios Avanzados for the PaMx33, PaMx35, PaMx41, and PaMx43 phages. We thank Dr. Aaron Whiteley at the University of Colorado, Boulder for his technical expertise and knowledge of CD-NTases and cyclic oligonucleotides.

We thank members of the Feng Lab, including Zhengyu Gao and Hao Wang, for their comprehensive efforts, technical expertise, and knowledge on structural and biochemical biology. We thank the staff at beamlines BL02U1 and BL19U1 of the Shanghai Synchrotron Radiation Facility for their assistance with data collection. We thank the Tsinghua University Branch of China National Center for Protein Sciences Beijing and Dr. Shilong Fan for providing facility support for X-ray diffraction of the crystal samples. We thank Drs. Yu Xiao and Teng Gao for their help with structure determination. We thank Drs. Yuanyuan Chen, Zhenwei Yang, and Bingxue Zhou at the Institute of Biophysics, Chinese Academy of Sciences for technical help with ITC experiments.

E.H. is supported by the National Science Foundation Graduate Research Fellowship Program (grant no. 2038436). Any opinions, findings, and conclusions or recommendations expressed in this material are those of the authors and do not necessarily reflect the views of the National Science Foundation. J.S.A. is supported by an EMBO Fellowship (ALTF 1201-2020). S.S. is supported by the Damon Runyon Fellowship Award (2352-19). Y. F. is supported by the National Natural Science Foundation of China (32171274). J.S.F. is supported by the National Institutes of Health (R35GM145238). J.B.-D. is supported by the National Institutes of Health (R21AI168811 and R01GM127489), the Vallee Foundation, and the Searle Scholarship.

AUTHOR CONTRIBUTIONS

E.H. conceived the project, designed and performed all *in vivo* experiments, and wrote the manuscript. X.C., Z.L., and N.A. purified the proteins. X.C. grew and optimized the crystals, collected the diffraction data, and performed the biochemical experiments. J.S.A. assisted with *in vitro* experiments. S.S. and H.C. contributed to execution and analysis of the whole-genome sequencing data. J.R. performed the HPLC analysis. Y.Z. performed the analysis of the binding characteristics of the ligands. J.S.F. performed the computational modeling and analysis of the phage capsid proteins. Y.F. designed and supervised the structural and mechanistic studies of Acb2, solved the crystal structure, analyzed the data, and wrote part of the manuscript. J.B.-D. supervised the project, designed experiments, and wrote the manuscript.

DECLARATION OF INTERESTS

J.B.-D. is a scientific advisory board member of SNIPR Biome, Excision Biotherapeutics, and LeapFrog Bio, and a scientific advisory board member and co-founder of Acrigen Biosciences. The Bondy-Denomy lab receives research support from Felix Biotechnology.

INCLUSION AND DIVERSITY

We support inclusive, diverse, and equitable conduct of research.

Received: January 13, 2022
Revised: October 29, 2022
Accepted: December 21, 2022
Published: February 6, 2023

REFERENCES

1. Barbalat, R., Ewald, S.E., Mouchess, M.L., and Barton, G.M. (2011). Nucleic acid recognition by the innate immune system. Annu. Rev. Immunol. *29*, 185–214. https://doi.org/10.1146/annurev-immunol-031210-101340.
2. Margolis, S.R., Wilson, S.C., and Vance, R.E. (2017). Evolutionary origins of cGAS-STING signaling. Trends Immunol. *38*, 733–743. https://doi.org/10.1016/j.it.2017.03.004.
3. Li, X.-D., Wu, J., Gao, D., Wang, H., Sun, L., and Chen, Z.J. (2013). Pivotal roles of cGAS-cGAMP signaling in antiviral defense and immune adjuvant effects. Science *341*, 1390–1394. https://doi.org/10.1126/science.1244040.
4. Wu, J., Sun, L., Chen, X., Du, F., Shi, H., Chen, C., and Chen, Z.J. (2013). Cyclic GMP-AMP is an endogenous second messenger in innate immune signaling by cytosolic DNA. Science *339*, 826–830. https://doi.org/10.1126/science.1229963.
5. Ishikawa, H., and Barber, G.N. (2008). STING is an endoplasmic reticulum adaptor that facilitates innate immune signalling. Nature *455*, 674–678. https://doi.org/10.1038/nature07317.
6. Burdette, D.L., Monroe, K.M., Sotelo-Troha, K., Iwig, J.S., Eckert, B., Hyodo, M., Hayakawa, Y., and Vance, R.E. (2011). STING is a direct innate immune sensor of cyclic di-GMP. Nature *478*, 515–518. https://doi.org/10.1038/nature10429.
7. Whiteley, A.T., Eaglesham, J.B., de Oliveira Mann, C.C., Morehouse, B.R., Lowey, B., Nieminen, E.A., Danilchanka, O., King, D.S., Lee, A.S.Y., Mekalanos, J.J., and Kranzusch, P.J. (2019). Bacterial cGAS-like enzymes synthesize diverse nucleotide signals. Nature *567*, 194–199. https://doi.org/10.1038/s41586-019-0953-5.
8. Cohen, D., Melamed, S., Millman, A., Shulman, G., Oppenheimer-Shaanan, Y., Kacen, A., Doron, S., Amitai, G., and Sorek, R. (2019). Cyclic GMP-AMP signalling protects bacteria against viral infection. Nature *574*, 691–695. https://doi.org/10.1038/s41586-019-1605-5.
9. Lau, R.K., Ye, Q., Patel, L., Berg, K.R., Mathews, I.T., Watrous, J.D., Whiteley, A.T., Lowey, B., Mekalanos, J.J., Kranzusch, P.J., et al. (2019). Structure and mechanism of a cyclic trinucleotide-activated bacterial endonuclease mediating bacteriophage immunity. Mol. Cell *77*. 723.e6–733.e6. https://doi.org/10.1016/j.molcel.2019.12.010.
10. Lowey, B., Whiteley, A.T., Keszei, A.F.A., Morehouse, B.R., Mathews, I.T., Antine, S.P., Cabrera, V.J., Kashin, D., Niemann, P., Jain, M., et al. (2020). CBASS immunity uses CARF-related effectors to sense 3′-5′- and 2′-5′-linked cyclic oligonucleotide signals and protect bacteria from phage infection. Cell *182*, 38–49.e17. https://doi.org/10.1016/j.cell.2020.05.019.
11. Duncan-Lowey, B., McNamara-Bordewick, N.K., Tal, N., Sorek, R., and Kranzusch, P.J. (2021). Effector-mediated membrane disruption controls cell death in CBASS antiphage defense. Mol. Cell *81*. 5039.e5–5051.e5. https://doi.org/10.1016/j.molcel.2021.10.020.
12. Morehouse, B.R., Yip, M.C.J., Keszei, A.F.A., McNamara-Bordewick, N.K., Shao, S., and Kranzusch, P.J. (2022). Cryo-EM structure of an active bacterial TIR-STING filament complex. Nature *608*, 803–807. https://doi.org/10.1038/s41586-022-04999-1.
13. Millman, A., Melamed, S., Amitai, G., and Sorek, R. (2020). Diversity and classification of cyclic-oligonucleotide-based anti-phage signalling systems. Nat. Microbiol. *5*, 1608–1615. https://doi.org/10.1038/s41564-020-0777-y.
14. Ye, Q., Lau, R.K., Mathews, I.T., Birkholz, E.A., Watrous, J.D., Azimi, C.S., Pogliano, J., Jain, M., and Corbett, K.D. (2020). HORMA domain proteins and a Trip13-like ATPase regulate bacterial cGAS-like enzymes to mediate bacteriophage immunity. Mol. Cell *77*. 709.e7–722.e7. https://doi.org/10.1016/j.molcel.2019.12.009.
15. Ledvina, H.E., Ye, Q., Gu, Y., Quan, Y., Lau, R.K., Zhou, H., Corbett, K.D., and Whiteley, A.T. (2022). cGASylation by a bacterial E1-E2 fusion protein primes antiviral immune signaling. 03.31.486616. https://doi.org/10.1101/2022.03.31.486616.
16. Jenson, J.M., Li, T., Du, F., and Chen, Z.J. (2022). Ubiquitin-like conjugation by bacterial cGAS enhances anti-phage defense https://doi.org/10.21203/rs.3.rs-1578554/v1.
17. Hobbs, S.J., Wein, T., Lu, A., Morehouse, B.R., Schnabel, J., Leavitt, A., Yirmiya, E., Sorek, R., and Kranzusch, P.J. (2022). Phage anti-CBASS and anti-Pycsar nucleases subvert bacterial immunity. Nature *605*, 522–526. https://doi.org/10.1038/s41586-022-04716-y.
18. Eaglesham, J.B., Pan, Y., Kupper, T.S., and Kranzusch, P.J. (2019). Viral and metazoan poxins are cGAMP-specific nucleases that restrict cGAS-STING signalling. Nature *566*, 259–263. https://doi.org/10.1038/s41586-019-0928-6.
19. Csörgő, B., León, L.M., Chau-Ly, I.J., Vasquez-Rifo, A., Berry, J.D., Mahendra, C., Crawford, E.D., Lewis, J.D., and Bondy-Denomy, J. (2020). A compact Cascade-Cas3 system for targeted genome engineering. Nat. Methods *17*, 1183–1190. https://doi.org/10.1038/s41592-020-00980-w.
20. Ha, A.D., and Denver, D.R. (2018). Comparative genomic analysis of 130 bacteriophages infecting bacteria in the genus Pseudomonas. Front. Microbiol. *9*, 1456. https://doi.org/10.3389/fmicb.2018.01456.
21. Guan, J., Oromí-Bosch, A., Mendoza, S.D., Karambelkar, S., Berry, J., and Bondy-Denomy, J. (2022). RNA targeting with CRISPR-Cas13a facilitates bacteriophage genome engineering. https://www.nature.com/articles/s41564-022-01243-4. https://doi.org/10.1101/2022.02.14.480438.
22. Athukoralage, J.S., McMahon, S.A., Zhang, C., Grüschow, S., Graham, S., Krupovic, M., Whitaker, R.J., Gloster, T.M., and White, M.F. (2020). An anti-CRISPR viral ring nuclease subverts type III CRISPR immunity. Nature *577*, 572–575. https://doi.org/10.1038/s41586-019-1909-5.
23. Holm, L. (2022). Dali server: structural unification of protein families. Nucleic Acids Res. *50*, W210–W215. https://doi.org/10.1093/nar/gkac387.
24. Cruz-Plancarte, I., Cazares, A., and Guarneros, G. (2016). Genomic and transcriptional mapping of PaMx41, archetype of a new lineage of bacteriophages infecting Pseudomonas aeruginosa. Appl. Environ. Microbiol. *82*, 6541–6547. https://doi.org/10.1128/AEM.01415-16.
25. Leavitt, A., Yirmiya, E., Amitai, G., Lu, A., Garb, J., Herbst, E., Morehouse, B.R., Hobbs, S.J., Antine, S.P., Sun, Z.-Y.J., et al. (2022). Viruses inhibit TIR gcADPR signaling to overcome bacterial defence. Nature *611*, 326–331. https://doi.org/10.1038/s41586-022-05375-9.
26. Li, L., Yin, Q., Kuss, P., Maliga, Z., Millán, J.L., Wu, H., and Mitchison, T.J. (2014). Hydrolysis of 2′3′-cGAMP by ENPP1 and design of nonhydrolyzable analogs. Nat. Chem. Biol. *10*, 1043–1048. https://doi.org/10.1038/nchembio.1661.
27. Eaglesham, J.B., and Kranzusch, P.J. (2020). Conserved strategies for pathogen evasion of cGAS-STING immunity. Curr. Opin. Immunol. *66*, 27–34. https://doi.org/10.1016/j.coi.2020.04.002.
28. Tal, N., Morehouse, B.R., Millman, A., Stokar-Avihail, A., Avraham, C., Fedorenko, T., Yirmiya, E., Herbst, E., Brandis, A., Mehlman, T., et al. (2021). Cyclic CMP and cyclic UMP mediate bacterial immunity against phages. Cell *184*. 5728.e16–5739.e16. https://doi.org/10.1016/j.cell.2021.09.031.
29. Zhang, T., Tamman, H., Coppieters 't Wallant, K., Kurata, T., LeRoux, M., Srikant, S., Brodiazhenko, T., Cepauskas, A., Talavera, A., Martens, C., et al. (2022). Direct activation of a bacterial innate immune system by a viral capsid protein. Nature *612*, 132–140. https://doi.org/10.1038/s41586-022-05444-z.
30. Yu, Y.T., and Snyder, L. (1994). Translation elongation factor Tu cleaved by a phage-exclusion system. Proc. Natl. Acad. Sci. USA *91*, 802–806. https://doi.org/10.1073/pnas.91.2.802.
31. Stokar-Avihail, A., Fedorenko, T., Garb, J., Leavitt, A., Millman, A., Shulman, G., Wojtania, N., Melamed, S., Amitai, G., and Sorek, R. (2022). Discovery of phage determinants that confer sensitivity to bacterial immune systems https://doi.org/10.1101/2022.08.27.505566.
32. Gao, L.A., Wilkinson, M.E., Strecker, J., Makarova, K.S., Macrae, R.K., Koonin, E.V., and Zhang, F. (2022). Prokaryotic innate immunity through

pattern recognition of conserved viral proteins. Science *377*, eabm4096. https://doi.org/10.1126/science.abm4096.

33. Garb, J., Lopatina, A., Bernheim, A., Zaremba, M., Siksnys, V., Melamed, S., Leavitt, A., Millman, A., Amitai, G., and Sorek, R. (2022). Multiple phage resistance systems inhibit infection via SIR2-dependent NAD^+ depletion. Nat. Microbiol. *7*, 1849–1856. https://doi.org/10.1038/s41564-022-01207-8.

34. Tesson, F., Hervé, A., Mordret, E., Touchon, M., d'Humières, C., Cury, J., and Bernheim, A. (2022). Systematic and quantitative view of the antiviral arsenal of prokaryotes. Nat. Commun. *13*, 2561. https://doi.org/10.1038/s41467-022-30269-9.

35. Johnson, M.C., Laderman, E., Huiting, E., Zhang, C., Davidson, A., and Bondy-Denomy, J. (2022). Core Defense Hotspots within Pseudomonas aeruginosa are a consistent and rich source of anti-phage defense systems https://doi.org/10.1101/2022.11.11.516204.

36. Cady, K.C., Bondy-Denomy, J., Heussler, G.E., Davidson, A.R., and O'Toole, G.A. (2012). The CRISPR/Cas adaptive immune system of Pseudomonas aeruginosa mediates resistance to naturally occurring and engineered phages. J. Bacteriol. *194*, 5728–5738. https://doi.org/10.1128/JB.01184-12.

37. Kropinski, A.M. (2000). Sequence of the genome of the temperate, serotype-converting, Pseudomonas aeruginosa bacteriophage D3. J. Bacteriol. *182*, 6066–6074. https://doi.org/10.1128/JB.182.21.6066-6074.2000.

38. Ceyssens, P.-J., Miroshnikov, K., Mattheus, W., Krylov, V., Robben, J., Noben, J.-P., Vanderschraeghe, S., Sykilinda, N., Kropinski, A.M., Volckaert, G., et al. (2009). Comparative analysis of the widespread and conserved PB1-like viruses infecting Pseudomonas aeruginosa. Environ. Microbiol. *11*, 2874–2883. https://doi.org/10.1111/j.1462-2920.2009.02030.x.

39. Essoh, C., Latino, L., Midoux, C., Blouin, Y., Loukou, G., Nguetta, S.P., Lathro, S., Cablanmian, A., Kouassi, A.K., Vergnaud, G., and Pourcel, C. (2015). Investigation of a large collection of Pseudomonas aeruginosa bacteriophages collected from a single environmental source in Abidjan, Côte d'Ivoire. PLoS One *10*, e0130548. https://doi.org/10.1371/journal.pone.0130548.

40. Pourcel, C., Midoux, C., Latino, L., Petit, M.-A., and Vergnaud, G. (2016). Complete genome sequences of Pseudomonas aeruginosa phages vB_PaeP_PcyII-10_P3P1 and vB_PaeM_PcyII-10_PII10A. Genome Announc. *4*, e00916-16. https://doi.org/10.1128/genomeA.00916-16.

41. Mesyanzhinov, V.V., Robben, J., Grymonprez, B., Kostyuchenko, V.A., Bourkaltseva, M.V., Sykilinda, N.N., Krylov, V.N., and Volckaert, G. (2002). The genome of bacteriophage phiKZ of Pseudomonas aeruginosa. J. Mol. Biol. *317*, 1–19. https://doi.org/10.1006/jmbi.2001.5396.

42. Monson, R., Foulds, I., Foweraker, J., Welch, M., and Salmond, G.P.C. (2011). The Pseudomonas aeruginosa generalized transducing phage phiPA3 is a new member of the phiKZ-like group of "jumbo" phages, and infects model laboratory strains and clinical isolates from cystic fibrosis patients. Microbiology (Reading) *157*, 859–867. https://doi.org/10.1099/mic.0.044701-0.

43. Lee, Y.J., Dai, N., Walsh, S.E., Müller, S., Fraser, M.E., Kauffman, K.M., Guan, C., Corrêa, I.R., Jr., and Weigele, P.R. (2018). Identification and biosynthesis of thymidine hypermodifications in the genomic DNA of widespread bacterial viruses. Proc. Natl. Acad. Sci. USA *115*, E3116–E3125. https://doi.org/10.1073/pnas.1714812115.

44. Ceyssens, P.J., Mesyanzhinov, V., Sykilinda, N., Briers, Y., Roucourt, B., Lavigne, R., Robben, J., Domashin, A., Miroshnikov, K., Volckaert, G., and Hertveldt, K. (2008). The genome and structural proteome of YuA, a new Pseudomonas aeruginosa phage resembling M6. J. Bacteriol. *190*, 1429–1435. https://doi.org/10.1128/JB.01441-07.

45. Lood, C., Danis-Wlodarczyk, K., Blasdel, B.G., Jang, H.B., Vandenheuvel, D., Briers, Y., Noben, J.-P., van Noort, V., Drulis-Kawa, Z., and Lavigne, R. (2020). Integrative omics analysis of Pseudomonas aeruginosa virus PA5oct highlights the molecular complexity of jumbo phages. Environ. Microbiol. *22*, 2165–2181. https://doi.org/10.1111/1462-2920.14979.

46. Bondy-Denomy, J., Pawluk, A., Maxwell, K.L., and Davidson, A.R. (2013). Bacteriophage genes that inactivate the CRISPR/Cas bacterial immune system. Nature *493*, 429–432. https://doi.org/10.1038/nature11723.

47. Bondy-Denomy, J., Qian, J., Westra, E.R., Buckling, A., Guttman, D.S., Davidson, A.R., and Maxwell, K.L. (2016). Prophages mediate defense against phage infection through diverse mechanisms. ISME J. *10*, 2854–2866. https://doi.org/10.1038/ismej.2016.79.

48. Ceyssens, P.J., Lavigne, R., Mattheus, W., Chibeu, A., Hertveldt, K., Mast, J., Robben, J., and Volckaert, G. (2006). Genomic analysis of Pseudomonas aeruginosa phages LKD16 and LKA1: establishment of the φKMV subgroup within the T7 supergroup. J. Bacteriol. *188*, 6924–6931. https://doi.org/10.1128/JB.00831-06.

49. Lammens, E., Ceyssens, P.-J., Voet, M., Hertveldt, K., Lavigne, R., and Volckaert, G. (2009). Representational difference analysis (RDA) of bacteriophage genomes. J. Microbiol. Methods *77*, 207–213. https://doi.org/10.1016/j.mimet.2009.02.006.

50. Lavigne, R., Burkal'tseva, M.V., Robben, J., Sykilinda, N.N., Kurochkina, L.P., Grymonprez, B., Jonckx, B., Krylov, V.N., Mesyanzhinov, V.V., and Volckaert, G. (2003). The genome of bacteriophage phiKMV, a T7-like virus infecting Pseudomonas aeruginosa. Virology *312*, 49–59. https://doi.org/10.1016/s0042-6822(03)00123-5.

51. Ceyssens, P.J., Brabban, A., Rogge, L., Lewis, M.S., Pickard, D., Goulding, D., Dougan, G., Noben, J.-P., Kropinski, A., Kutter, E., and Lavigne, R. (2010). Molecular and physiological analysis of three Pseudomonas aeruginosa phages belonging to the "N4-like viruses.". Virology *405*, 26–30. https://doi.org/10.1016/j.virol.2010.06.011.

52. Choi, K.-H., and Schweizer, H.P. (2006). mini-Tn7 insertion in bacteria with single attTn7 sites: example Pseudomonas aeruginosa. Nat. Protoc. *1*, 153–161. https://doi.org/10.1038/nprot.2006.24.

53. Choi, K.-H., Mima, T., Casart, Y., Rholl, D., Kumar, A., Beacham, I.R., and Schweizer, H.P. (2008). Genetic tools for select-agent-compliant manipulation of Burkholderia pseudomallei. Appl. Environ. Microbiol. *74*, 1064–1075. https://doi.org/10.1128/AEM.02430-07.

54. Shanks, R.M.Q., Caiazza, N.C., Hinsa, S.M., Toutain, C.M., and O'Toole, G.A. (2006). Saccharomyces cerevisiae-based molecular tool kit for manipulation of genes from gram-negative bacteria. Appl. Environ. Microbiol. *72*, 5027–5036. https://doi.org/10.1128/AEM.00682-06.

55. Sayers, E.W., Bolton, E.E., Brister, J.R., Canese, K., Chan, J., Comeau, D.C., Connor, R., Funk, K., Kelly, C., Kim, S., et al. (2022). Database resources of the national center for biotechnology information. Nucleic Acids Res. *50*, D20–D26. https://doi.org/10.1093/nar/gkab1112.

56. Chen, I.-M.A., Chu, K., Palaniappan, K., Ratner, A., Huang, J., Huntemann, M., Hajek, P., Ritter, S., Varghese, N., Seshadri, R., et al. (2021). The IMG/M data management and analysis system v.6.0: new tools and advanced capabilities. Nucleic Acids Res. *49*, D751–D763. https://doi.org/10.1093/nar/gkaa939.

57. Abby, S.S., Néron, B., Ménager, H., Touchon, M., and Rocha, E.P.C. (2014). MacSyFinder: a program to mine genomes for molecular systems with an application to CRISPR-Cas systems. PLoS One *9*, e110726. https://doi.org/10.1371/journal.pone.0110726.

58. Madeira, F., Pearce, M., Tivey, A.R.N., Basutkar, P., Lee, J., Edbali, O., Madhusoodanan, N., Kolesnikov, A., and Lopez, R. (2022). Search and sequence analysis tools services from EMBL-EBI in 2022. Nucleic Acids Res. *50*, W276–W279. https://doi.org/10.1093/nar/gkac240.

59. Papadopoulos, J.S., and Agarwala, R. (2007). COBALT: constraint-based alignment tool for multiple protein sequences. Bioinformatics *23*, 1073–1079. https://doi.org/10.1093/bioinformatics/btm076.

60. Letunic, I., and Bork, P. (2018). 20 years of the SMART protein domain annotation resource. Nucleic Acids Res. *46*, D493–D496. https://doi.org/10.1093/nar/gkx922.

61. Steinegger, M., and Söding, J. (2017). MMseqs2 enables sensitive protein sequence searching for the analysis of massive data sets. Nat. Biotechnol. *35*, 1026–1028. https://doi.org/10.1038/nbt.3988.

62. Martin, M. (2011). Cutadapt removes adapter sequences from high-throughput sequencing reads. EMBnet J. *17*, 10–12. https://doi.org/10.14806/ej.17.1.200.

63. Langmead, B., and Salzberg, S.L. (2012). Fast gapped-read alignment with Bowtie 2. Nat. Methods *9*, 357–359. https://doi.org/10.1038/nmeth.1923.

64. Zimmermann, L., Stephens, A., Nam, S.-Z., Rau, D., Kübler, J., Lozajic, M., Gabler, F., Söding, J., Lupas, A.N., and Alva, V. (2018). A completely reimplemented MPI bioinformatics toolkit with a new HHpred server at its core. J. Mol. Biol. *430*, 2237–2243. https://doi.org/10.1016/j.jmb.2017.12.007.

65. Jumper, J., Evans, R., Pritzel, A., Green, T., Figurnov, M., Ronneberger, O., Tunyasuvunakool, K., Bates, R., Žídek, A., Potapenko, A., et al. (2021). Highly accurate protein structure prediction with AlphaFold. Nature *596*, 583–589. https://doi.org/10.1038/s41586-021-03819-2.

66. Otwinowski, Z., and Minor, W. (1997). Processing of X-ray diffraction data collected in oscillation mode. Methods Enzymol. *276*, 307–326. https://doi.org/10.1016/S0076-6879(97)76066-X.

67. Adams, P.D., Grosse-Kunstleve, R.W., Hung, L.W., Ioerger, T.R., McCoy, A.J., Moriarty, N.W., Read, R.J., Sacchettini, J.C., Sauter, N.K., and Terwilliger, T.C. (2002). PHENIX: building new software for automated crystallographic structure determination. Acta Crystallogr. D Biol. Crystallogr. *58*, 1948–1954. https://doi.org/10.1107/s0907444902016657.

68. Emsley, P., Lohkamp, B., Scott, W.G., and Cowtan, K. (2010). Features and development of coot. Acta Crystallogr. D Biol. Crystallogr. *66*, 486–501. https://doi.org/10.1107/S0907444910007493.

69. Qiu, D., Damron, F.H., Mima, T., Schweizer, H.P., and Yu, H.D. (2008). PBAD-based shuttle vectors for functional analysis of toxic and highly regulated genes in Pseudomonas and Burkholderia spp. and other bacteria. Appl. Environ. Microbiol. *74*, 7422–7426. https://doi.org/10.1128/AEM.01369-08.

70. Edgar, R.C. (2004). MUSCLE: multiple sequence alignment with high accuracy and high throughput. Nucleic Acids Res. *32*, 1792–1797. https://doi.org/10.1093/nar/gkh340.

71. Hmelo, L.R., Borlee, B.R., Almblad, H., Love, M.E., Randall, T.E., Tseng, B.S., Lin, C., Irie, Y., Storek, K.M., Yang, J.J., et al. (2015). Precision-engineering the Pseudomonas aeruginosa genome with two-step allelic exchange. Nat. Protoc. *10*, 1820–1841. https://doi.org/10.1038/nprot.2015.115.

72. Robinson, J.T., Thorvaldsdóttir, H., Winckler, W., Guttman, M., Lander, E.S., Getz, G., and Mesirov, J.P. (2011). Integrative genomics viewer. Nat. Biotechnol. *29*, 24–26. https://doi.org/10.1038/nbt.1754.

73. Meeske, A.J., Jia, N., Cassel, A.K., Kozlova, A., Liao, J., Wiedmann, M., Patel, D.J., and Marraffini, L.A. (2020). A phage-encoded anti-CRISPR enables complete evasion of type VI-A CRISPR-Cas immunity. Science *369*, 54–59. https://doi.org/10.1126/science.abb6151.

74. Rouillon, C., Athukoralage, J.S., Graham, S., Grüschow, S., and White, M.F. (2019). Investigation of the cyclic oligoadenylate signaling pathway of type III CRISPR systems. Methods Enzymol *616*, 191–218.

75. Marino, N.D., Zhang, J.Y., Borges, A.L., Sousa, A.A., Leon, L.M., Rauch, B.J., Walton, R.T., Berry, J.D., Joung, J.K., Kleinstiver, B.P., and Bondy-Denomy, J. (2018). Discovery of widespread type I and type V CRISPR-Cas inhibitors. Science *362*, 240–242. https://doi.org/10.1126/science.aau5174.

76. Desper, R., and Gascuel, O. (2004). Theoretical foundation of the balanced minimum evolution method of phylogenetic inference and its relationship to weighted least-squares tree fitting. Mol. Biol. Evol. *21*, 587–598. https://doi.org/10.1093/molbev/msh049.

Please cite this article in press as: Huiting et al., Bacteriophages inhibit and evade cGAS-like immune function in bacteria, Cell (2023), https://doi.org/10.1016/j.cell.2022.12.041

STAR★METHODS

KEY RESOURCES TABLE

REAGENT or RESOURCE	SOURCE	IDENTIFIER
Bacterial and virus strains		
P. aeruginosa ATCC 33351 WT	ATCC	NCBI: AWZD00000000.1
P. aeruginosa JD332	Jeremy R. Dettman Lab	NCBI: LJNX01000000.1
P. aeruginosa BWH058	Deborah Hung Lab	NCBI: JIES00000000.1
P. aeruginosa ATCC 27853 WT	ATCC	NCBI: CP015117.1
P. aeruginosa BWHPSA011 (Pa011) WT	Deborah Hung Lab	NCBI: NZ_AXQR00000000.1
Pa011 ΔCBASS (Removal of 1250436-1254723bp; *CapV, CdnA, Cap2, Cap3, DUF2188*)	This study	N/A
Pa011 CapV (phospholipase) catalytic mutant S48A	This study	N/A
Pa011 CdnA (cyclase) catalytic mutant D87A/D89A	This study	N/A
Pa011 Cap 2 (E1/E2) catalytic mutant C450A/C453A	This study	N/A
Pa011 Cap3 (JAB) catalytic mutant E38A	This study	N/A
P. aeruginosa PAO1 (Pa) WT	Joe Bondy-Denomy Lab	NCBI: NC_002516.2
Pa^{CBASS} (PAO1 *att*Tn7::Pa011 CBASS; *CapV, CdnA, Cap2, Cap3, DUF2188*)	This study	N/A
Pa^{EV} (Integration of mini-Tn7 empty vector)	This study	N/A
Pa^{CBASS} (JBD67 WT) lysogen	This study	N/A
Pa^{CBASS} (JBD67Δ*acb2*) lysogen	This study	N/A
Pa^{EV} (JBD67 WT) lysogen	This study	N/A
Pa^{EV} (JBD67Δ*acb2*) lysogen	This study	N/A
Pa^{haCas3} (PAO1 *att*Tn7::I-C CRISPR-Cas3 helicase attenuated (haCas3) system)	This study	N/A
Pa^{Cas13a} (PAO1 *att*Tn7::VI-A CRISPR-Ca13a system)	Joe Bondy-Denomy Lab[21]	N/A
E. coli DH5α	NEB	Cat #C2987H
E. coli SM10	NEB	Cat #C3019H
E. coli BL21 (DE3)	Weidi Biotechnology	Cat #EC1002
PaMx33	Gabriel Guarneros Peña Lab[24]	NCBI: KU884561
PaMx35	Gabriel Guarneros Peña Lab[24]	NCBI: KU884562
PaMx41	Gabriel Guarneros Peña Lab[24]	NCBI: KU884563
PaMx43	Gabriel Guarneros Peña Lab[24]	NCBI: KU884564
JBD18	Alan Davidson Lab[36]	NCBI: JX495041.1
JBD67	Alan Davidson Lab[36]	NCBI: NC_042135.1
JBD67Δ*acb2* #1 (Removal of 23005-23232bp *orf34*)	This study	N/A
JBD67Δ*acb21* #2 (Removal of 23047-23235bp *orf34*)	This study	N/A
JBD67Δ*acb2* #3 (Removal of 23066-23239bp *orf34*)	This study	N/A
D3	Alan Davison Lab[37]	NCBI: AF165214.2
PB-1	Alan Davison Lab[38]	NCBI: NC_011810
F8	Alan Davison Lab[38]	NCBI: NC_011703

(*Continued on next page*)

Continued

REAGENT or RESOURCE	SOURCE	IDENTIFIER
14-1	Alan Davison Lab[38]	NCBI: NC_007810
Lind109	Alan Davison Lab	N/A
Ab27	Christine Pourcel Lab[39]	NCBI: LN610579
Ab28	Christine Pourcel Lab[39]	NCBI: LN610589
PII10A	Christine Pourcel Lab[40]	NCBI: LT594786
PhiKZ	Alan Davison Lab[41]	NCBI: AF399011
PA3	Alan Davison Lab[42]	NCBI: HQ630627
Ab03	Christine Pourcel Lab[39]	NCBI: LN610573
Ab04	Christine Pourcel Lab[39]	NCBI: LN610581
Ab06	Christine Pourcel Lab[39]	NCBI: LN610582
Ab11	Christine Pourcel Lab[39]	NCBI: LN610583
Ab17	Christine Pourcel Lab[39]	NCBI: LN610576
M6	Peter Weigele[43]	NCBI: NC_007809
YuA	Rob Lavigne Lab[44]	NCBI: NC_010116
Ab18	Christine Pourcel Lab[39]	NCBI: LN610577
Ab19	Christine Pourcel Lab[39]	NCBI: NC_042115
Ab20	Christine Pourcel Lab[39]	NCBI: LN610585
Ab21	Christine Pourcel Lab[39]	NCBI: NC_042115
PA5oct	Rob Lavigne Lab[45]	NCBI: MK797984
PA-1	Peter Weigele[43]	NCBI: MN504636.1
DMS3	Alan Davison Lab[36]	NCBI: DQ631426.1
JBD25	Alan Davison Lab[36]	NCBI: JX495042.1
JBD30	Alan Davison Lab[46]	NCBI: NC_020198.1
Ab30	Christine Pourcel Lab[39]	NCBI: LN610590
JBD68	Alan Davison Lab[47]	NCBI: KY707339.1
LKD16	Rob Lavigne Lab[48]	NCBI: AM265638
LKD19	Rob Lavigne Lab[49]	NCBI: AM910651
KMV	Rob Lavigne Lab[50]	NCBI: AJ505558
Ab05	Christine Pourcel Lab[39]	NCBI: LN610574
Ab12	Christine Pourcel Lab[39]	NCBI: NC_047967
LUZ7	Rob Lavigne Lab[51]	NCBI: NC_013691.1
Lit1	Rob Lavigne Lab[51]	NCBI: NC_013692.1
Ab09	Christine Pourcel Lab[39]	NCBI: HG962375
P3P1	Christine Pourcel Lab[40]	NCBI: LT594787
Ab22	Christine Pourcel Lab[39]	NCBI: LN610578
Chemicals, peptides, and recombinant proteins		
HEPES sodium salt	Sigma-Aldrich	CAS: 7365-45-9 Cat #V900477-500G
Tris base	Sigma-Aldrich	CAS: 77-86-1 Cat #RDD008-2.5KG
Sodium dihydrogen phosphate dihydrate	Sigma-Aldrich	CAS: 13472-35-0 Cat #1063420250
Disodium hydrogen phosphate dodecahydrate	Sigma-Aldrich	CAS: 10039-32-4 Cat #1065790500
Bis-Tris propane	Sigma-Aldrich	CAS: 64431-96-5 Cat #B6755-25G
Sodium bromide	Sigma-Aldrich	CAS: 7647-15-6 Cat #310506-100G

(*Continued on next page*)

Please cite this article in press as: Huiting et al., Bacteriophages inhibit and evade cGAS-like immune function in bacteria, Cell (2023), https://doi.org/10.1016/j.cell.2022.12.041

Continued

REAGENT or RESOURCE	SOURCE	IDENTIFIER
PEG 3350	Biorigin	CAS: 25322-68-3 Cat #BN33640
Ethylene glycol	Sigma-Aldrich	CAS: 107-21-1 Cat #102466
Glycerol	Sigma-Aldrich	CAS: 56-81-5 Cat#V900122-500ML
Imidazole	Sigma-Aldrich	CAS: 288-32-4 Cat #V900153-500G
Resorufin butyrate	CHEMEGEN	CAS: 15585-42-9 Cat #CY17497
Phenol:chloroform:isoamyl alcohol 25:24:1	Sigma-Aldrich	CAS: 108-95-2; 67-66-3; 123-51-3 Cat #P3803
Chloroform	Sigma-Aldrich	CAS: 67-66-3 Cat #C2432
Lysozyme	Sigma-Aldric	CAS: 12650-88-3 Cat #L6876
2X Phanta Max Master Mix	Vazyme	Cat #P515-03
2X Rapid Taq Master Mix	Vazyme	Cat #P222-AA
Gibson Assembly HiFi DNA Master Mix	NEB	Cat #E2621
KOD-Plus-Neo	TOYOBO	Cat #KOD-401
DpnI	NEB	Cat #R0176s
SacI	NEB	Cat #R3156S
PstI	NEB	Cat #R3140S
HindIII	NEB	Cat #R3104S
BamHI	NEB	Cat #R3136S
Proteinase K	NEB	Cat #P8107S
RnaseA	Omega Bio-TEK	Cat #AC118
ATP	NEB	Cat #P0756S
PNK Buffer	NEB	Cat #B0201S
T4 PNK	NEB	Cat #M0201S
Ligase Buffer	NEB	Cat #B0202S
T4 Ligase	NEB	Cat #M0202S
High Affinity Ni-NTA Resin	GenScript	Cat #L00250-100
Pa011 CdnA recombinant protein	This study	N/A
Pa011 CapV recombinant protein	This study	N/A
Pa011 Cap2 (E1/E2) recombinant protein	This study	N/A
Pa011 Cap2$^{C105A/C479A}$ recombinant protein	This study	N/A
P1011 CdnA-Cap2$^{C105A/C479A}$ recombinant protein	This study	N/A
PaMx33 Acb2 WT recombinant protein	This study	N/A
PaMx33 Acb2^{Y11A} recombinant protein	This study	N/A
PaMx33 Acb2^{K26A} recombinant protein	This study	N/A
Critical commercial assays		
DNA Clean & Concentrator Kit	Zymo Research	Cat #D4034
Gel DNA Recovery Kit	Zymo Research	Cat #D4008
Plasmid Miniprep Kit	Zymo Research	Cat #ZD4037
Qubit 1X dsDNA High Sensitivity Assay Kit	ThermoFisher	Cat #Q33231
Illumina DNA Prep Kit	Illumina	Cat #20015825
Illumina Miseq v3 Reagents	Illumia	Cat #15043894
Plasmid Miniprep Kit	Vazyme	Cat #DC201-01

(*Continued on next page*)

Please cite this article in press as: Huiting et al., Bacteriophages inhibit and evade cGAS-like immune function in bacteria, Cell (2023), https://doi.org/10.1016/j.cell.2022.12.041

Continued

REAGENT or RESOURCE	SOURCE	IDENTIFIER
Gel DNA Extraction Mini Kit	Vazyme	Cat #DC301-01
LFS Crystallization Screen Kit	Molecular Dimensions	Cat #MD1-121
3',3' cyclic GAMP ELISA Kit	Arbor Assays	Cat #K073-H1
Deposited data		
Structure of Acb2	This study	PDB: 8H2X
Structure of Acb2 bound with 3',3'-cGAMP	This study	PDB: 8H2J
Structure of Acb2 bound with c-di-AMP	This study	PDB: 8H39
Oligonucleotides		
PaMx41 *orf11* crRNA guide #4: gatacgaccagtctgacgcttgac	This study	N/A
PaMx41 *orf11* crRNA guide #5: tctgacgcttgacggtaagattga	This study	N/A
JBD67 *orf34* crRNA guide #3: Tctgacgcttgacggtaagattga	This study	N/A
JBD67 *orf34* crRNA guide #4: ctggctgcagagccgttgcgctgg gctgcgatcg	This study	N/A
3',3'-cGAMP	Sigma-Aldrich	CAS: 849214-04-6 Cat #SML1232-.5UMO
2',3'-cGAMP	Sigma-Aldrich	CAS:1441190-66-4 Cat #SML1229-.5UMO
c-di-GMP	Sigma-Aldrich	CAS: 61093-23-0 Cat #SML1228-1UMO
c-di-AMP	Sigma-Aldrich	CAS: 54447-84-6 Cat #SML1231-1UMO
3',3'-c-UMP-GMP	Biolog Life Science Institute	CAS: 232933-52-7 Cat #C371
3',3'-c-di-UMP	Biolog Life Science Institute	CAS: 73120-97-5 Cat #C256
3',3'-c-UMP-AMP	Biolog Life Science Institute	CAS: 83799-66-0 Cat #C357
Recombinant DNA		
pHERD30T (p30T)	Qiu et al.[51]	N/A
p30T-Pa011 CBASS	This study	N/A
p30T-PaMx41-short orf24-v1 (37 a.a. with stop codon)	This study	N/A
p30T-PaMx41-short orf24-v2 (94 a.a. with stop codon)	This study	N/A
p30T-PaMx41-long orf24 (*acb2*)	This study	N/A
p30T-HDR-Acb2-AcrVIA1	This study	N/A
p30T-crRNA-4-PaMx41-orf11	This study	N/A
p30T-crRNA-5-PaMx41-orf11	This study	N/A
p30T-crRNA-3-JBD67-orf34	This study	N/A
p30T-crRNA-4-JBD67-orf34	This study	N/A
pUC18-mini-Tn7T-LAC (pTn7)	Choi and Schweizer[52]	N/A
pTn7-Pa011 CBASS	This study	N/A
pTNS3	Choi et al.[53]	N/A
pMQ30	Shanks et al.[54]	N/A
pMQ30-HDR-Pa011-CapV-S48A	This study	N/A
pMQ30-HDR-Pa011-CdnA-D87A-D89A	This study	N/A
pMQ30-HDR-Pa011-E1-E2-C450A-C453A	This study	N/A
pMQ30-HDR-Pa011-JAB-E38A	This study	N/A
p30T-PaMx41-orf11-HDR-1-WT	This study	N/A
p30T-PaMx41-orf11-HDR-2-WT	This study	N/A
p30T-PaMx41-orf11-I121S	This study	N/A

(*Continued on next page*)

Please cite this article in press as: Huiting et al., Bacteriophages inhibit and evade cGAS-like immune function in bacteria, Cell (2023), https://doi.org/10.1016/j.cell.2022.12.041

Continued

REAGENT or RESOURCE	SOURCE	IDENTIFIER
p30T-PaMx41-orf11-I121T	This study	N/A
p30T-PaMx41-orf11-S330P	This study	N/A
p30T-PaMx41-Acb2-Y11A	This study	N/A
p30T-PaMx41-Acb2-K26A	This study	N/A
pET28a- His_6-SUMO-Acb2	This study	N/A
pET28a- His_6-SUMO-Acb2-Y11A	This study	N/A
pET28a- His_6-SUMO-Acb2-K26A	This study	N/A
pET28a-His_6-CapV	This study	N/A
pET28a-His_6-CdnA	This study	N/A
pET28a-His_6-Cap2 E1/E2	This study	N/A
pET28a- His_6-Cap2 E1/E2-C105A/C479A	This study	N/A
pRSFDuet- His_6-CdnA-Cap2 E1/E2-C105A/C479A	This study	N/A
Software and algorithms		
National Center for Biotechnology Information (NCBI) database	Sayers et al.[55]	https://blast.ncbi.nlm.nih.gov/
Integrated Microbial Genomes (IMG) database	Chen et al.[56]	https://img.jgi.doe.gov/
DefenseFinder	Tesson et al.[34] and Abby et al.[57]	https://defense-finder.mdmparis-lab.com/
Multiple Sequence Comparison by Log-Expectation (MUSCLE)	Madeira et al.[58]	https://www.ebi.ac.uk/Tools/msa/muscle/
NCBI Multiple Sequence Alignment Viewer (MSA)	MSA Software	https://www.ncbi.nlm.nih.gov/tools/msaviewer/
NCBI Constraint-based Multiple Alignment Tool (COBALT)	Papadopoulos and Agarwala[59]	https://www.ncbi.nlm.nih.gov/tools/cobalt/re_cobalt.cgi
Interactive Tree of Life (iTOL)	Letunic et al.[60]	https://itol.embl.de/
MMSeqs2	Steinegger and Söding[61]	https://github.com/soedinglab/mmseqs2
Cutadapt	Martin[62]	https://cutadapt.readthedocs.io/en/stable/#
Bowtie2	Langmead and Salzberg[63]	https://bowtie-bio.sourceforge.net/bowtie2/index.shtml
Integrative Genomics Viewer (IGV)	Robinson et al.[63]	https://software.broadinstitute.org/software/igv/
SeqDiff	SeqDiff GitHub Program	https://github.com/hansenlo/SeqDiff
HHpred	Zimmermann et al.[64]	https://toolkit.tuebingen.mpg.de/tools/hhpred
AlphaFold2	Jumper et al.[65]	https://alphafold.ebi.ac.uk/
DALI	Holm[23]	http://ekhidna2.biocenter.helsinki.fi/dali/
HKL2000	Otwinowski and Minor[66]	http://www.hkl-xray.com/
PHENIX	Adams et al.[67]	http://www.phenix-online.org
COOT	Emsley et al.[68]	http://www2.mrc-lmb.cam.ac.uk/personal/pemsley/coot
PyMOL	The PyMOL Molecular Graphics System, Version 2.5.2., Schrodinger, LLC	https://pymol.org/2/
OriginPro 8	OriginPro Software	N/A
GraphPad Prism 9	GraphPad Software	https://www.graphpad.com/
Other		
Amicon Ultra-0.5 centrifugal filter unit	Merck	Cat #UFC500396
Lysing Matrix B beads	MP	Cat #6911100
Amicon concentrators (3 K)	Millipore	Cat #UFC800308
Amicon concentrators (10 K)	Millipore	Cat #UFC901096
Amicon concentrators (30 K)	Millipore	Cat #UFC903024

(*Continued on next page*)

Please cite this article in press as: Huiting et al., Bacteriophages inhibit and evade cGAS-like immune function in bacteria, Cell (2023), https://doi.org/10.1016/j.cell.2022.12.041

Continued

REAGENT or RESOURCE	SOURCE	IDENTIFIER
HisTrap FF (5 mL)	GE Healthcare	Cat #17-5255-01
HiTrap Heparin HP (5 mL)	GE Healthcare	Cat #17-0407-03
HiTrap Q Sepharose FF (5 mL)	GE Healthcare	Cat #17-5156-01
Superdex 200 increase 10/300 GL	GE Healthcare	Cat #17517501

RESOURCE AVAILABILITY

Lead contact

Further information and requests for resources and reagents should be directed to and will be fulfilled by the lead contact, Joseph Bondy-Denomy (Joseph.Bondy-Denomy@ucsf.edu).

Materials availability

All unique/stable reagents generated in this study are available from the Lead Contact with a completed Materials Transfer Agreement.

Data and code availability

The accession number for the coordinate and structure factors reported in this paper is PDB: 8H2X (Acb2), 8H2J (Acb2-3',3'-cGAMP) and 8H39 (Acb2-c-di-AMP). This paper does not report original code. Any additional information required to reanalyze the data reported in this paper is available from the Lead Contact upon request.

EXPERIMENTAL MODEL AND SUBJECT DETAILS

Bacterial strains and phages

The bacterial strains and phages used in this study are listed in the key resources table. The *P. aeruginosa* strains (ATCC 33351, JD332, BWHPSA011, BWH058, ATCC 27853, PAO1) and *E. coli* strains (DH5α and SM10) were grown in Lysogeny broth (LB) medium at 37°C both with aeration at 225 r.p.m. Plating was performed on LB solid agar with 10 mM $MgSO_4$ when performing phage infections, and when indicated, gentamicin (50 μg ml^{-1} for *P. aeruginosa* and 15 μg ml^{-1} for *E. coli*) was used to maintain the pHERD30T plasmid. Gene expression was induced by the addition of L-arabinose (0.01% final for BWHPSA011 bacterial genes and 0.1% for phage genes, unless otherwise specified).

The *E. coli* BL21 (DE3) strain was used for recombinant protein overexpression and grown in Lysogeny broth (LB) medium. The cells were grown at 37°C until OD_{600nm} reached 0.8 and then induced at 18°C for 12 h.

METHOD DETAILS

Identification of CBASS operons

tBLASTn was used to query the amino acid sequence of eight known CD-NTases (CdnA-H) against sequenced *Pseudomonas aeruginosa* genomes contained in the NCBI[55] and IMG[56] databases as well as our sequenced UCSF clinical isolates. Proteins with >25% amino acid sequence identity to a validated CD-NTase were accepted as "hits"[7], leading to the identification of >300 CBASS operons in 252 distinct *P. aeruginosa* strains. The *P. aeruginosa* BWHPSA011 (Pa011) strain contains a Type II-A CBASS operon in contig 12 (NCBI Genome ID: NZ_AXQR000000012.1) ranging from 1250439-1254679bp, with CapV (phospholipase effector, NCBI Gene ID: Q024_30602), CdnA (cyclase, Q024_30601), Cap2 (E1/E2, Q024_30600), and Cap3 (JAB, intergenic region 1250439-1250912bp).

Identification of anti-phage immune systems

DefenseFinder was used to systematically identify all known anti-phage bacterial immune system operons in *P. aeruginosa* strains,[34,57] and the output was used to construct the table in Figure 1A.

Episomal gene expression

The shuttle vector that replicates in *P. aeruginosa* and *E. coli*, pHERD30T[69] was used for cloning and episomal expression of genes in *P. aeruginosa* BWHPSA011 (Pa011) or PAO1 strains. This vector has an arabinose-inducible promoter and a selectable gentamicin marker. Vector was digested with SacI and PstI restriction enzymes and purified. Inserts were amplified by PCR using bacterial overnight culture or phage lysate as the DNA template, and joined into the pHERD30T vector at the SacI-PstI restriction enzyme cut sites by Hi-Fi DNA Gibson Assembly (NEB) following the manufacturer's protocol. The resulting plasmids were transformed into *E. coli* DH5α. All plasmid constructs were verified by sequencing using primers that annealed to sites outside the multiple cloning site. *P. aeruginosa* cells were electroporated with the pHERD30T constructs and selected on gentamicin.

Please cite this article in press as: Huiting et al., Bacteriophages inhibit and evade cGAS-like immune function in bacteria, Cell (2023), https://doi.org/10.1016/j.cell.2022.12.041

Site-directed mutagenesis

Site-directed mutagenesis (SDM) of the pHERD30T constructs introduced mutations in the acb2 gene that were not found naturally in the phages and therefore could not be amplified via PCR. Primers were designed so that the forward primer encompassed the nucleotide mutations and the reverse primer directly adjacent. Primers were subjected to a T4 PNK phosphorylation reaction and then around-the-world PCR was performed. The linearized plasmid was confirmed on a gel, subjected to DpnI digestion to remove parent wild-type plasmid, and then purified. A T4 DNA ligase reaction was performed and resulting plasmids were used for transformations and sequenced verified.

Chromosomal CBASS integration

For chromosomal insertion of the Pa011 CBASS operon, the integrating vector pUC18-mini-Tn7T-LAC[52] and the transposase expressing helper plasmid pTNS3[53] were used to insert the BWHPSA011 CBASS operon at the Tn7 locus in *P. aeruginosa* PAO1 strain (Pa^{CBASS}), or an pUC18-mini-Tn7T-LAC empty vector (E.V.) control strain (Pa^{EV}). The vector was linearized using around-the-world PCR, treated with DpnI, and then purified. Two overlapping inserts encompassing the CBASS operon were amplified by PCR using Pa011 overnight culture as the DNA template, and joined into the pUC18-mini-Tn7T-LAC vector a the SacI-PstI restriction enzyme cut sites by Hi-Fi DNA Gibson Assembly (NEB) following the manufacturer's protocol. The resulting plasmids were used to transform *E. coli* DH5α. All plasmid constructs were verified by sequencing using primers that annealed to sites outside the multiple cloning site. *P. aeruginosa* PAO1 cells were electroporated with pUC18-mini-Tn7T-LAC and pTNS3 and selected for on gentamicin. Potential integrants were screened by colony PCR with primers PTn7R and PglmS-down, and then verified by sequencing using primers that anneal to sites outside the attTn7 site. Electrocompetent cell preparations, transformations, integrations, selections, plasmid curing, and FLP-recombinase-mediated marker excision with pFLP were performed as described previously.[52]

Chromosomal mutants of *P. aeruginosa* BWHPSA011

The allelic exchange vector that replicates in P. aeruginosa and E. coli, pMQ30[54] was used for generating the chromosomal CBASS knockout and CBASS mutant genes in *P. aeruginosa* BWHPSA011 (Pa011). Vector was digested with HindIII and BamHI restriction enzymes and purified. For the CBASS knockout strain, homology arms >500bp up- and downstream of CBASS operon were amplified by PCR using Pa011 overnight culture as the template DNA. For the CBASS gene mutant strains, homology arms >500bp up- and downstream of CBASS gene catalytic residue(s), with the appropriate mutant nucleotides, were amplified by PCR using Pa011 overnight culture as the template DNA. Previously identified catalytic residues in *Escherichia coli* TW11681 (NZ_AELD01000000)[8] were used to aid the identification of the catalytic residues in *Pseudomonas aeruginosa* BWHPSA011. Multiple Sequence Comparison by Log-Expectation (MUSCLE,[70] and NCBI Multiple Sequence Alignment Viewer (MSA) were subsequently used to validate conserved catalytic residues between *P. aeruginosa* BWHPSA011, *Vibrio cholerae* El Tor N16961 (NC_002505.1), and *E.coli* TW11681. The inserts were joined into the pMQ30 vector at the HindIII-BamHI restriction enzyme cut sites by Hi-Fi DNA Gibson Assembly (NEB) following the manufacturer's protocol. The resulting plasmids were transformed into *E. coli* DH5α. All plasmid constructs were verified by sequencing using primers that annealed to sites outside the multiple cloning site. *E. coli* SM10 cells were electroporated with pMQ30 constructs and selected for on gentamicin. *E. coli* SM10 harboring the pMQ30 construct were mated with Pa011 to transfer the plasmid and enable allelic exchange. Potential mutant Pa011 strains were subjected to a phenotype cross streak screen with PaMx41-like phages and then verified by sequencing using primers that anneal to sites outside of the homology arms. Electrocompetent cell preparations, transformations, selections, and plasmid curing were performed as described previously.[71]

Phage growth

All phages were grown at 37°C with solid LB agar plates containing 20 ml of bottom agar containing 10 mM $MgSO_4$ and any necessary inducers or antibiotics. Phages were initially grown on the permissible host *P. aeruginosa* PAO1 WT, which naturally lacks CBASS. 150 μl of overnight cultures of PAO1 were infected with 10 μl of low titer phage lysate (>10^{4-7} pfu/ml) and then mixed with 3 ml of 0.7% top agar 10 mM $MgSO_4$ for plating on the LB solid agar. After incubating at 37°C overnight, individual phage plaques were picked from top agar and resuspended in 200 μl SM phage buffer. For high titer lysates, the purified phage was further amplified on LB solid agar plates with PAO1 WT. After incubating 37°C overnight, SM phage buffer was added until the solid agar lawn was completely covered and then incubated for 5-10 minutes at room temperature. The whole cell lysate was collected and a 1% volume of chloroform was added, and then left to shake gently on an orbital shaker at room temperature for 15 min followed by centrifugation at maximum g for 3 min to remove cell debris. The supernatant phage lysate was stored at 4°C for downstream assays.

Plaque assays

Plaque assays were conducted at 37°C with solid LB agar plates. 150 μl of overnight bacterial culture was mixed with top agar and plated. Phage lysates were diluted 10-fold then 2 μl spots were applied to the top agar after it had been poured and solidified.

Lysogen construction with JDB67 phage

Lysogens were constructed by spotting serial dilutions of JDB67 WT or JBD67Δ*acb2* phage lysates on the engineered *P. aeruginosa* PAO1 strain that harbors BWHPSA011 CBASS in the chromosome (Pa^{CBASS}), or a mini-Tn7 E.V. control (Pa^{EV}) strain, and streaking out the bacteria (that is, putative lysogens) from the inside of the clearing resulting from a clutter of plaques onto a solid LB agar plate.

Colonies were then screened using a cross streak test to confirm resistance to the phage used to lysogenize the strain. The putative lysogens were grown in liquid culture, and the presence of spontaneously produced phage in the supernatant that could plaque on the PAO1 wildtype strain confirmed lysogeny.

Isolation of CBASS phage escapers

For identifying PaMx41 WT phage escapers of CBASS, 150 μl of overnight cultures of the *P. aeruginosa* strain BWHPSA011 (Pa011) were infected with 10 μl of high titer phage lysate (>10^9 pfu/ml) and then plated on LB solid agar. After incubating at 37°C overnight, 10 individual phage plaques were picked from top agar and resuspended in 200 μl SM phage buffer. Phage lysates were purified for three rounds using the CBASS expressing strain. Three PaMx41 WT control phages were picked, purified, and propagated in parallel by infecting the Pa011 ΔCBASS strain. To validate the phage identity, PCR and Sanger sequencing were performed on nucleotide sequences unique to PaMx41.

To identify PaMx41 *Δacb2*, JBD67 *Δacb2*, and JBD18 WT phage escapers of CBASS, 150 μl of overnight cultures of the CBASS expressing strains (Pa011 WT or Pa^{CBASS}) were infected with 10 μl of high titer phage lysate (>10^9 pfu/ml) and plated on LB solid agar. After incubating at 37°C overnight, no obvious plaques were observed. SM phage buffer was added to the entire lawn and whole cell lysate collected. Next, to propagate the mutant escaper phage population, 150 μl of overnight cultures of the *P. aeruginosa* strains lacking CBASS (Pa011 ΔCBASS or Pa^{EV}) were infected with 10 μl of the phage lysates and plated on LB solid agar. After incubating at 37°C overnight, SM phage buffer was added to the entire lawn and whole cell lysate collected. Lastly, to isolate individual escaper plaques, 150 μl of overnight cultures of the CBASS expressing strains (Pa011 WT or Pa^{CBASS}) were infected with 10 μl of the previously collected phage lysate and plated on LB solid agar After incubating at 37°C overnight, at least four individual phage plaques were picked from top agar and resuspended in 200 μl SM phage buffer. Phage lysates were purified for three rounds using the CBASS expressing strain. At least two control or WT phages were picked, purified, and propagated in parallel by infecting the Pa011 ΔCBASS or Pa^{EV} strains. To validate the phage identity, PCR and Sanger sequencing were performed on nucleotide sequences unique to each phage.

Whole genome sequencing (WGS) and analysis

Genomic DNA from phage lysates was extracted using a modified SDS/Proteinase K method. Briefly, 200 μL high titer phage lysate (>10^9 pfu/ml) was mixed with an equal volume of lysis buffer (10 mM Tris, 10 mM EDTA, 100 μg/mL proteinase K, 100 μg/mL RNaseA, 0.5% SDS) and incubated at 37°C for 30 min, and then 55°C for 30 min. Preps were further purified using the DNA Clean & Concentrator Kit (Zymo Research). DNA was quantified using the Qubit 4.0 Fluorometer (Life Technologies). 20-100 ng genomic DNA was used to prepare WGS libraries using the Illumina DNA Prep Kit (formerly known as Illumina Nextera Flex Kit) using a modified protocol that utilized 5x reduced quantities of tagmentation reagents per prep, except for the bead washing step with Tagment Wash Buffer (TWB), where the recommended 100 μL of TWB was used. Subsequent on-bead PCR indexing-amplification of tagmented DNA was performed using 2x Phusion Master Mix (NEB) and custom-ordered indexing primers (IDT) matching the sequences from the Illumina Nextera Index Kit. Each 50 μL reaction was split in two tubes, amplified for 9 and 12 cycles respectively. Libraries were further purified by agarose gel electrophoresis; DNA was excised around the ~400 bp size range and purified using the Zymoclean Gel DNA Recovery Kit (Zymo Research). Libraries were quantified by Qubit and the 9-cycle reaction was used unless the yield was too low for sequencing, in which case the 12-cycle reaction was used. Libraries were pooled in equimolar ratios and sequenced with Illumina MiSeq v3 reagents (150 cycles, Read 1; 8 cycles, Index 1; 8 cycles, Index 2). WGS data were demultiplexed either on-instrument or using a custom demultiplexing Python script (written by Dr. Nimit Jain), and trimmed using cutadapt (v 3.4[62]) to remove Nextera adapters. Trimmed reads were mapped using Bowtie 2.0 (–very-sensitive-local alignments[63]) and alignments were visualized using IGV (v 2.9.4[72]). Variants were detected using the SeqDiff program (https://github.com/hansenlo/SeqDiff).

CRISPR-Cas13a phage gene editing

Construction of template plasmids for homologous recombination and selection of engineered phages via the CRISPR-Cas13a system were performed as described previously.[21] Specifically, homology arms of >500bp up- and downstream of PaMx41 *acb2* were amplified by PCR using Pamx41 WT phage genomic DNA as the template. The *acrVIA1* gene was amplified from plasmid pAM383,[73] a gift from Luciano Marraffini, The Rockefeller University. PCR products were purified and assembled as a recombineering substrate and then inserted into the NheI site of the pHERD30T vector. The resulting plasmids were electroporated into *P. aeruginosa* PAO1 cells. PAO1 strains carrying the recombination plasmid were grown in LB media supplemented with gentamicin. 150 μl of overnight cultures were infected with 10 μl of high titer phage lysate (>10^9 pfu/ml; PaMx33 WT, PaMx35 WT, PaMx43 WT, PaMx41 ESC or PaMx41 WT) and then plated on LB solid agar. After incubating at 37°C overnight, SM phage buffer was added to the entire lawn and whole cell lysate collected. The resulting phage lysate containing both WT and recombinant phages were tittered on PAO1 strains with a chromosomally integrated Type VI-A CRISPR-Cas13a system, and the most efficiently targeting crRNA guide (specific to *orf11*; guide #5) was used to screen for recombinants. PAO1 strains carrying the Cas13a system and crRNA of choice were grown overnight in LB media supplemented with gentamicin. 150 μl of overnight cultures were infected with 10 μl of low titer phage lysate (10^{4-7} pfu/ml), and then plated onto LB solid agar containing 0.3% arabinose and 1 mM isopropyl β-d-1-thiogalactopyranoside (IPTG). After incubating at 37°C overnight, individual phage plaques were picked from top agar and resuspended in 200 μl SM phage buffer. Phage lysates were purified for three rounds using the Cas13a counter-selection strain (guide #5), and further propagated on a

complementary Cas13a counter-selection strain (guide #4), to select against Cas13a escaper phages. To determine whether the phages were recombinants, PCR was performed with the appropriate pairs of primers amplifying the region outside of the homology arms, an internal region of *acrVIA1*, and *acb2*.

Homologous recombination-mediated mutation of phage gene

Construction of template plasmids for homologous recombination consisted of homology arms >500bp up- and downstream of the mutation of interest encoded in PaMx41 *orf11*. The homology arms were amplified by PCR using PaMx41Δ*acb2* escapers phage genomic DNA as the template, and PaMx41 WT phage genomic DNA as the control template. Template 1 primers were designed to symmetrically flank the PaMx41 *orf11* mutations I121S and I121T, and template 2 primers were designed to symmetrically flank mutation I327T and S330P. PCR products were purified and assembled as a recombineering substrate and then inserted into the SacI-PstI site of the pHERD30T vector. The resulting plasmids were electroporated into *P. aeruginosa* BWHPSA011 (Pa011) ΔCBASS cells. Pa011 strains carrying the recombination plasmid were grown in LB media supplemented with gentamicin. 150 μl of overnight cultures were infected with 10 μl of high titer phage lysate (>10^9 pfu/ml; PaMx41Δ*acb2*) and then plated on LB solid agar. After incubating at 37°C overnight, SM phage buffer was added to the entire lawn and whole cell lysate collected. The resulting phage lysate containing both WT and recombinant phages were screened on a lawn of Pa011 WT cells harboring an active CBASS system. Specifically, 150 μl of overnight Pa011 WT cultures were infected with 10 μl of low titer phage lysate (10^{4-7} pfu/ml), and then plated onto LB solid agar. After incubating at 37°C overnight, individual phage plaques were picked from top agar and resuspended in 200 μl SM phage buffer. Phage lysates were purified for three rounds using the Pa011 WT strain. To confirm whether the phages were recombinants, PCR was performed with the appropriate pairs of primers amplifying the region outside of the homology arms and subject to Sanger Sequencing.

Helicase attenuated Cas3 removal of phage genes

Cas3 (Type I-C)-specific guides targeting JBD67 *acb2* were cloned into a pHERD30T-derived vector containing modified I-C repeats as previously described.[19] The guides electroporated into *P. aeruginosa* PAO1 strains with a chromosomally integrated Type I-C helicase attenuated Cas3 system. JBD67 WT phage lysate was tittered on the PAO1 strains and the efficiently targeting crRNA guide (specific to *acb2*; guide #3) was identified. PAO1 strains carrying the Type I-C CRISPR-Cas system with a helicase attenuated Cas3 enzyme and crRNA targeting phage JBD67 *acb2* were grown overnight in LB media supplemented with gentamicin. 150 μl of overnight cultures were infected with 10 μl of high titer phage lysate (>10^9 pfu/ml; JBD67) and plated on LB agar plates containing gentamicin, 0.1% arabinose, and 1 mM isopropyl β-d-1-thiogalactopyranoside (IPTG). After incubating at 37°C overnight, SM phage buffer was added to the entire lawn and whole cell lysate collected. The resulting phage lysate containing both WT and *acb2* knockout phages were grown on a complementary Cas3 counter-selection strain (guide #4) to select against Cas3 escaper phages. 150 μl of overnight cultures were infected with 10 μl of low titer phage lysate (10^{4-7} pfu/ml; JBD67 WT) and then plated on LB solid agar containing 0.1% arabinose and 1 mM IPTG. After incubating at 37°C overnight, individual phage plaques were picked from top agar and replica-plated onto LB solid agar with $PAO1^{EV}$ and $PAO1^{CBASS}$ strains. JDB67 plaque sizes that were reduced on the $PAO1^{CBASS}$ plate compared to the positive control (JBD18 WT phage) were identified as potential CBASS sensitive phages. Corresponding plaques on the $PAO1^{EV}$ plate were picked and resuspended in 200 μl SM phage buffer. To determine whether the phages harbored deletions in *acb2*, PCR was performed with the appropriate pairs of primers amplifying a ~1kb region outside of *acb2*.

Intracellular 3',3'-cGAMP measurements

Cell lysates were prepared similarly to previous methods,[8] in which *P. aeruginosa* BWHPA011 (Pa011) cells harboring a catalytically dead *capV* gene ($CapV^{S48A}$) were used and then transformed with a pHERD30T vector expressing *acb2* WT or K26A. Cells were taken from overnight culture, diluted 1:100 in 150ml LB medium with G50 and 0.1% arabinose (flask size 500ml), and then grown at 37°C (190 r.p.m.) until reaching an OD_{600nm} of 0.3-0.4. From the culture, 100 ml was aliquoted and 10 mM MgSO4 added. The cells were then infected with PaMx41Δ*acb2* to obtain an MOI of ~5 and ensure at least one or more phages were infecting each bacterial cell. After 60 minutes following infection, the culture was separated into two 50 ml samples and centrifuged at 7,500 g for 10 mins at 4°C. Following centrifugation, supernatant was removed and pellets were kept on ice until resuspended in 600 μl of phosphate buffer (50 mM sodium phosphate (pH 7.4), 300 mM NaCl, 10% (v/v) glycerol). The resuspended pellet was supplemented with 1 μl hen-lysozyme (Sigma-Aldrich), vortexed briefly, and incubated at 25°C for 10 min. The resuspended cells were then mixed with Lysing Matrix B (MP) beads and cells were disrupted mechanically using Mini-Beadbeater 16 Biospec Products (1 cycle of 2:30, 3,450 oscillations/m, at 4 °C). Cell lysates were then centrifuged at 17,500 g for 10 min at 4°C. For each condition, one 50 ml cell lysate and subsequent supernatant was (i) loaded onto a 3kDa filter (Amicon Ultra-0.5 centrifugal filter unit; Merk) and the corresponding 50 ml cell lysate and subsequent supernatant was (ii) subjected to phenol-chloroform/chloroform nucleotide extraction[74]. For the filtration step, the unit was centrifuged at 16,000 g for 45 min at 4 °C and flow-through (containing small molecules less than 3kDa) was used as the sample for 3',3'-cGAMP measurements. For the nucleotide extraction step, 600 μl of supernatant was added to 600 μl of phenol-chloroform, vortexed for 30 sec, and then centrifuged at 17,500 g for 45 min at 4 °C. The top aqueous layer was carefully transferred into another eppendorf tube and 600 μl of chloroform was added, vortexed for 30 sec, and then centrifuged at 17,500 g for 10 min at 4 °C. The top aqueous layer was added to the 3kD filter, centrifuged at 16,000 g for 45 min at 4 °C, and flow-through collected. Each flow-through sample was run in technical

triplicate on a 3',3'-cGAMP ELISA Kit (Arbor Assays) and standards were prepared in the same phosphate buffer. 3',3'-cGAMP concentrations were calculated using a sigmoidal standard curve via GraphPad Prism (v 9.4.1).

Phylogenetic analysis

Phylogenetic reconstructions were conducted similar to previous work in our lab.[75] Homologs of Acb2 were acquired through 3 iterations of psiBLASTp search the non-redundant protein database. Hits with >70% coverage and an E value <0.0005 were included in the generation of the position specific scoring matrix (PSSM). High confidence homologs (>70% coverage, E value < 0.0005) represented in unique species of bacteria were then aligned using NCBI COBALT[59] using default settings and a phylogeny was generated in Cobalt using the fastest minimum evolution method[76] employing a maximum sequence difference of 0.85 and Grishin distance to calculate the tree. The resulting phylogeny was then displayed as a phylogenetic tree using iTOL: Interactive Tree of Life.[60]

Computational modeling of phage capsid

Models of *P. aeruginosa* PaMx41 (orf11) and JBD18 (orf35) phage capsid proteins were generated using AlphaFold2[65] and aligned using the PyMol "super" function to the different chains of the *E. coli* T4 phage capsid structure (PDB: 6UZC).

Protein expression and purification

The Acb2, CapV, CdnA and Cap2 genes were synthesized by GenScript. The full-length Acb2 gene was amplified by PCR and cloned into a modified pET28a vector in which the expressed Acb2 protein contains a His-SUMO tag. The Acb2 mutants were generated by two-step PCR and were subcloned, overexpressed and purified in the same way as wild-type protein. The proteins were expressed in *E. coli* strain BL21 (DE3) and induced by 0.2 mM isopropyl-β-D-thiogalactopyranoside (IPTG) when the cell density reached an OD_{600nm} of 0.8. After growth at 18°C for 12 h, the cells were harvested, re-suspended in lysis buffer (50 mM Tris–HCl pH 8.0, 300 mM NaCl, 10 mM imidazole and 1 mM PMSF) and lysed by sonication. The cell lysate was centrifuged at 20,000 g for 50 min at 4°C to remove cell debris. The supernatant was applied onto a self-packaged Ni-affinity column (2 mL Ni-NTA, Genscript) and contaminant proteins were removed with wash buffer (50 mM Tris pH 8.0, 300 mM NaCl, 30 mM imidazole). The fusion protein was then digested with Ulp1 at 18°C for 2 h, and then the Acb2 protein was eluted with wash buffer. The eluant of Acb2 was concentrated and further purified using a Superdex-200 increase 10/300 GL (GE Healthcare) column equilibrated with a buffer containing 10 mM Tris-HCl pH 8.0, 200 mM NaCl and 5 mM DTT. The purified protein was analyzed by SDS-PAGE. The fractions containing the target protein were pooled and concentrated.

The CdnA, Cap2 and CdnA-Cap2 complex were purified as His-tagged proteins, which were eluted with elution buffer (50 mM Tris pH 8.0, 300 mM NaCl, 300 mM imidazole) after removing contaminant proteins with wash buffer. The cells expressing CapV were resuspended with lysis buffer containing 50 mM phosphate buffer pH 7.4, 300 mM NaCl, 10% glycerol (v/v). The CapV proteins bound to Ni-NTA beads were washed with a buffer containing 50 mM phosphate buffer pH 7.4, 300 mM NaCl, 10% glycerol (v/v), 30 mM imidazole and then eluted with the 50 mM phosphate buffer (pH 7.4), 300 mM NaCl, 10% glycerol (v/v), 300 mM imidazole. The eluant of CapV was concentrated and further purified using a Superdex-200 increase 10/300 GL (GE Healthcare) column equilibrated with a reaction buffer containing 50 mM phosphate buffer (pH 7.4), 300 mM NaCl, 10% glycerol (v/v). The purified protein was analyzed as described above.

Crystallization, data collection and structural determination

The Acb2 protein was concentrated to 24 mg/mL in 10 mM Tris-HCl pH 8.0, 200 mM NaCl and 5 mM DTT. Crystals were grown using the hanging-drop vapor diffusion method. Crystals of Acb2 were grown at 18°C by mixing an equal volume of the protein (24 mg/mL) with reservoir solution containing 0.2 M Sodium bromide, 0.1 M Bis-Tris propane pH 6.5, 10% Ethylene glycol and 20% v/v PEG 3350. Crystals of Acb2 in complex with 3',3'-cGAMP or c-di-AMP were grown under the same reservoir solution. Prior to crystallization, 3',3'-cGAMP or c-di-AMP were mixed with the protein at a molar ratio of 0.8:1. The crystals appeared overnight and grew to full size in about two to three days. The crystals were cryoprotected in the reservoir solution containing 20% glycerol before its transferring to liquid nitrogen.

All the data were collected at the X-ray crystallography facility at Tsinghua University (XtaLAB Synergy Custom FRX and a hybrid photon counting detector HyPix-6000, Rigaku, Japan) and SSRF beamlines BL02U1 and BL19U1, integrated and scaled using the HKL2000 package.[66] The initial model of Acb2 was obtained through modeling using AlphaFold2. [65] The structures of Acb2 and its complex with ligands were solved through molecular replacement and refined manually using COOT.[68] The structure was further refined with PHENIX[67] using non-crystallographic symmetry and stereochemistry information as restraints. The final structure was obtained through several rounds of refinement. Data collection and structure refinement statistics are summarized in Table S1.

Isothermal titration calorimetry binding assay

The dissociation constants of binding reactions of Acb2 or Acb2 mutants with the 3',3'-cGAMP/2',3'-cGAMP/c-di-GMP/c-di-AMP/3',3'-c-di-UMP/3',3'-c-UMP-AMP/3',3'-c-UMP-GMP were determined by isothermal titration calorimetry (ITC) using a MicroCal ITC200 calorimeter. Both proteins and cyclic dinucleotides were desalted into the working buffer (20 mM HEPES pH 7.5 and 200 mM NaCl). The titration was carried out with 19 successive injections of 2 μL cyclic dinucleotides at the 0.4 mM concentration,

Please cite this article in press as: Huiting et al., Bacteriophages inhibit and evade cGAS-like immune function in bacteria, Cell (2023), https://doi.org/10.1016/j.cell.2022.12.041

spaced 120 s apart, into the sample cell containing the Acb2 or Acb2 mutants with a concentration of 0.1 mM by 700 rpm at 25°C. The Origin software was used for baseline correction, integration, and curve fitting to a single site binding model.

Fluorogenic biochemical assay for CapV activity

The enzymatic reaction velocity was measured as previously described.[8] Briefly, the esterase activity of the 6×His-tagged CapV was probed with the fluorogenic substrate resorufin butyrate. The CapV protein was diluted in 50 mM sodium phosphate pH 7.4, 300 mM NaCl, 10% (v/v) glycerol to a final concentration of 1.77 μM. To determine the enzymatic activity of CapV activated by 3',3'-cGAMP, increasing concentrations ranging from 0.025 to 0.8 μM of 3',3'-cGAMP was added to DMSO solubilized resorufin butyrate (stock of 20 mM mixed with 50 mM sodium phosphate pH 7.4, 300 mM NaCl, 10% v/v glycerol reaching a final concentration of 100 μM). Subsequently, the purified 6×His-tagged CapV was added to the reaction solution containing 3',3'-cGAMP to a final assay volume of 50 μL, and fluorescence was measured in a 96-well plate (Corning 96-well half area black non-treated plate with a flat bottom). Plates were read once every 30 s for 20 min at 37°C using a EnSpire Multimode Plate Reader (PerkinElmer) with excitation and emission wavelengths of 550 and 591 nm, respectively. To determine the function of Acb2, 32 μM Acb2 and 0.8 μM 3',3'-cGAMP were pre-incubated at 18°C, and the subsequent detection method was as described above. To examine whether the released molecule from Acb2 is able to activate CapV, 0.8 μM 3',3'-cGAMP was incubated with 32 μM Acb2 for 10 min at 18°C. Proteinase K was subsequently added to the reaction system at a final concentration of 0.065 mg/mL and the reaction was performed at 58°C for 3 h. Reaction products were transferred to Amicon Ultra-4 Centrifugal Filter Unit 3 kDa and centrifuged at 4°C, 4,000 g. Filtered products were used for CapV activity assay.

Gel filtration assay

The Acb2, CapV, CdnA, Cap2 and the CdnA-Cap2 complex purified as described above were subjected to gel filtration analysis (Superdex-200 increase 10/300 GL, GE Healthcare). The Acb2 was incubated with CapV, CdnA, Cap2 or the CdnA-Cap2 complex at a molar ratio of 5:1 overnight on ice before the gel filtration analysis in buffer containing 10 mM Tris–HCl pH 8.0, 200 mM NaCl, and 5 mM DTT. The assays were performed with a flow rate of 0.5 mL/min and an injection volume of 1 mL for each run. Samples from relevant fractions were subjected to SDS-PAGE and visualized by Coomassie blue staining.

Analytical ultracentrifugation

Proteins were extensively dialyzed against AUC buffer (10 mM Tris pH 8.0, 200 mM NaCl). Sedimentation velocity studies were performed in a Beckman XL-A analytical ultracentrifuge at 20°C and 35,000 rpm. The absorbance at 280 nm was collected every 4 min for a total of 200 scans. These values were used to fit the data to the Lamm equation in SEDFIT software using the continuous *c*(s) distribution model. Graphs were prepared using Origin software.

Native-PAGE assay

Acb2 was pre-incubated with cyclic dinucleotides for 10 min at 18°C, where Acb2 was 14.3 μM and the concentrations of cyclic dinucleotides ranged from 1.8 to 7.2 μM (1.8, 3.6, 7.2 μM). Products of the reaction were analyzed using 5% native polyacrylamide gels and visualized by Coomassie blue staining.

High-performance liquid chromatography (HPLC)

40 μM Acb2 was pre-incubated with 4 μM 3',3'-cGAMP for 10 min at 18°C. Proteinase K was subsequently added to the reaction system at a final concentration of 0.25 mg/mL and the reaction was performed at 58°C for 1 h. Reaction products were transferred to Amicon Ultra-15 Centrifugal Filter Unit 3 kDa and centrifuged at 4°C, 4,000 g. The products obtained by filtration were further filtered with a 0.22 μm filter and subsequently used for HPLC experiments. The HPLC analysis was performed on an Agilent 1200 system with a ZORBAX Bonus-RP column (4.6 × 150 mm). A mixture of acetonitrile (2%) and 0.1% trifluoroacetic acid solution in water (98%) were used as mobile phase with 0.8 mL/min. The compounds were detected at 254 nm

QUANTIFICATION AND STATISTICAL ANALYSIS

Statistical details for each experiment can be found in the figure legends and outlined in the corresponding methods details section. Data are plotted with error bars representing standard deviation (s.d.).

CellPress
OPEN ACCESS

Supplemental figures

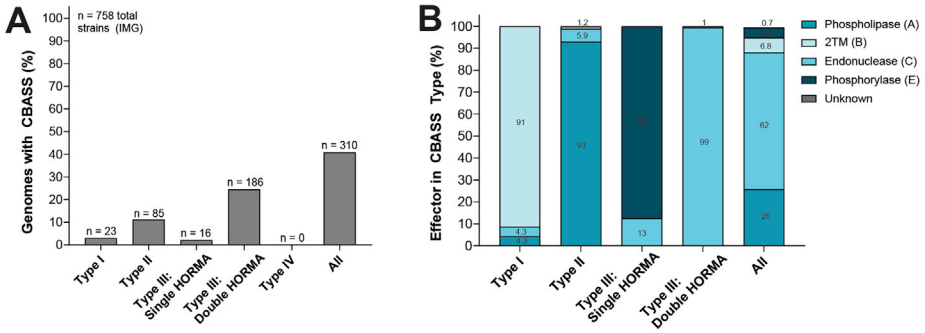

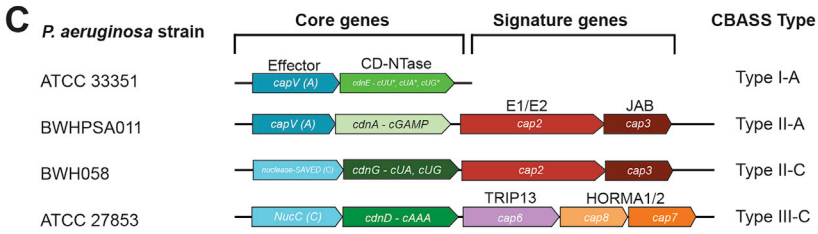

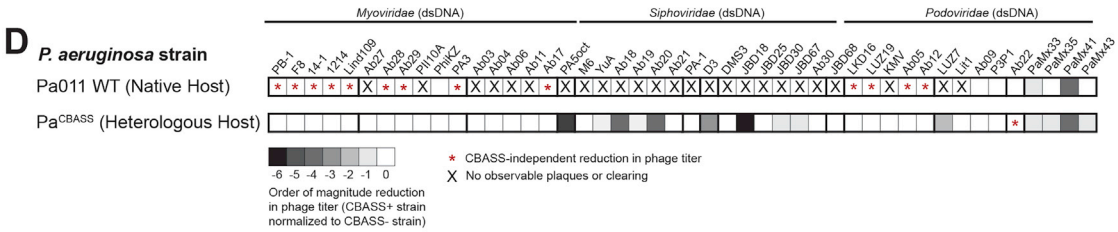

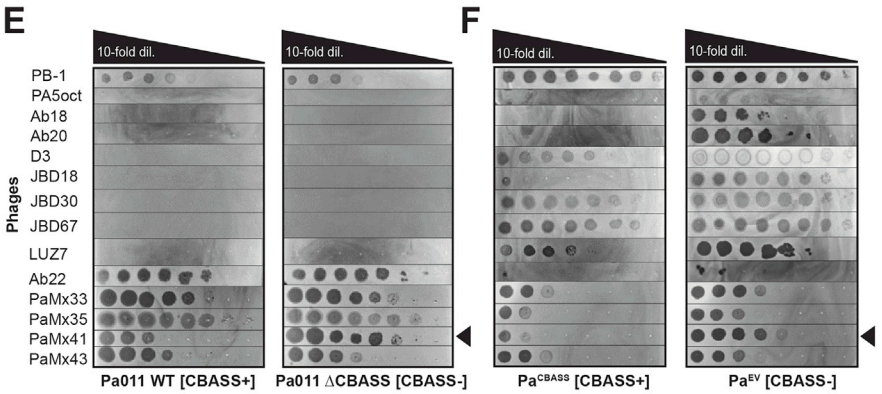

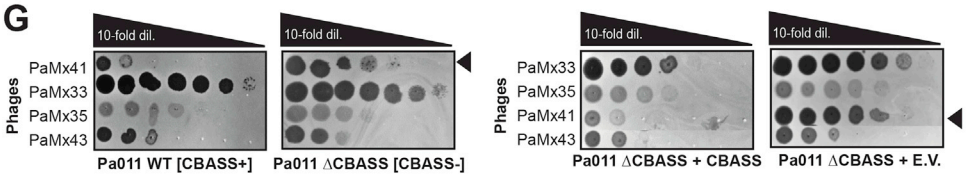

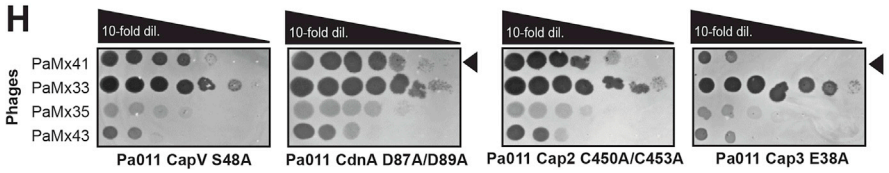

(legend on next page)

Figure S1. Diversity of CBASS in *Pseudomonas aeruginosa* strains and CBASS-dependent and -independent phage targeting, related to Figure 1

(A and B) (A) Percentage of *P. aeruginosa* genomes that encode a CBASS operon and (B) percentage of effector genes in each CBASS type. Data are shown for *P. aeruginosa* in the IMG database (n = 758); some genomes may encode more than one CBASS type/operon.

(C) The presence of different CBASS types in *P. aeruginosa* strains according to their operon composition of core and signature genes. Core genes include cGAS/DncV-like nucleotidyltransferase (CD-NTase) and effector genes. Known and predicted (*) cyclic nucleotides are denoted next to the CD-NTase gene.[7] Signature genes are denoted as CD-NTase-associated proteins (Cap).

(D) Heatmap representing the order of magnitude reduction in phage titer on a CBASS-encoding (Pa011 WT native CBASS host or Pa^{CBASS} heterologous CBASS host; CBASS+) strain normalized to a strain lacking CBASS (Pa011 ΔCBASS or Pa^{EV}; CBASS−). 46 (out of 64 total) phages infected one or both strains and are represented in the heatmap.

(E and F) (E) Plaque assays with indicated phages spotted in 10-fold serial dilutions on a lawn of Pa011 WT or ΔCBASS or (F) on a lawn of Pa^{CBASS} or Pa^{EV}, to highlight CBASS-dependent targeting and CBASS-independent targeting (PB-1 and Ab22 phages). Plaque assays were used to quantify the order of magnitude reduction in phage titer by comparing the number of spots (with plaques, or clearing if plaques were not visible) on the CBASS+ strain divided by the CBASS− strain (n = 3).

(G) Plaque assays with the indicated phages spotted in 10-fold serial dilutions on a lawn of Pa011 WT or ΔCBASS, and Pa011 ΔCBASS overexpressing the CBASS operon or empty vector (E.V.).

(H) Plaque assays on a lawn of Pa011 chromosomal mutants of each CBASS gene (*capV*^{S48A} [phospholipase], *cdnA*$^{D87A/D89A}$ [cyclase], *cap2*$^{C450A/C453A}$ [E1/E2], and *cap3*^{E38A} [JAB]). For all plaque assays, clearings represent phage replication, and black arrowheads highlight the reduction of PaMx41 WT phage titer.

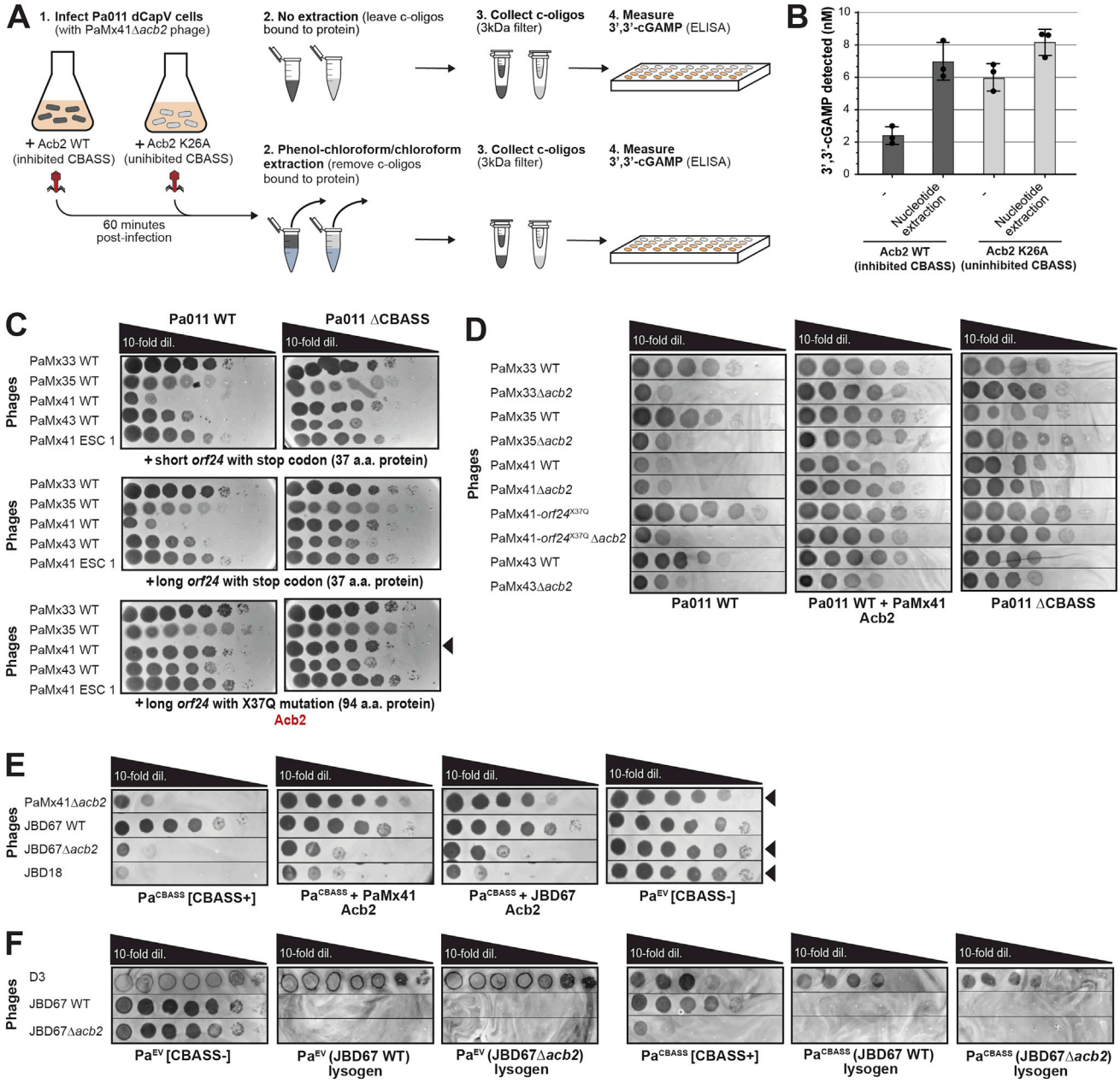

Figure S2. Acb2 protects phage and reduces 3′,3′-cGAMP molecules in CBASS-containing cells, related to Figures 1, 2, and 4

(A) Schematic of *in vivo* phage infection and cGAMP detection: (1) Pa011 cells with catalytically dead CapV^{S48A} strain overexpressing a wild-type version of an anti-CBASS gene (Acb2 WT; inhibited CBASS) or mutant version (Acb2 K26A; uninhibited or active CBASS). These cells are infected with PaMx41 phage that lacks Acb2 (PaMx41Δ*acb2*) at an MOI of ~5 for 60 min to provide the phage time to proceed through its replication cycle.[24] (2) Cell lysates are processed without (–) or with phenol-chloroform/chloroform nucleotide extraction. (3) Resultant lysates are filtered to collect cyclic oligonucleotides. (4) Then 3′,3′-cGAMP is specifically measured by an ELISA.

(B) 3′,3′-cGAMP detected in each respective condition performed in biological triplicate. Data are mean ± SD.

(C) Plaque assays were performed with PaMx33, 35, 41, and 43 WT phages, as well as an evolved PaMx41 CBASS escape (ESC) phage, spotted in 10-fold serial dilutions on a lawn of Pa011 WT [CBASS+] or ΔCBASS [CBASS–] overexpressing the indicated genes; black arrowhead highlights increase in PaMx41 WT phage titer.

(D) Plaque assays were performed with the indicated phages spotted in 10-fold serial dilutions on a lawn of Pa011 WT, ΔCBASS, or WT overexpressing *acb2*.

(E) Plaque assays with indicated phages on a lawn of *P. aeruginosa* cells (PAO1) with a chromosomally integrated Pa011 CBASS operon (Pa^{CBASS}), or empty vector (Pa^{EV}), and overexpressing *acb2*. Black arrowhead highlights CBASS-dependent change in phage titer.

(F) Plaque assays with the indicated phages spotted in 10-fold serial dilutions on a lawn of Pa^{EV} [CBASS–], Pa^{EV} (JBD67 WT) lysogen, or Pa^{EV} (JBD67Δ*acb2*) lysogen, or Pa^{CBASS} [CBASS+], Pa^{CBASS} (JBD67 WT) lysogen, or Pa^{CBASS} (JBD67Δ*acb2*) lysogen. For all plaque assays, clearings represent phage replication.

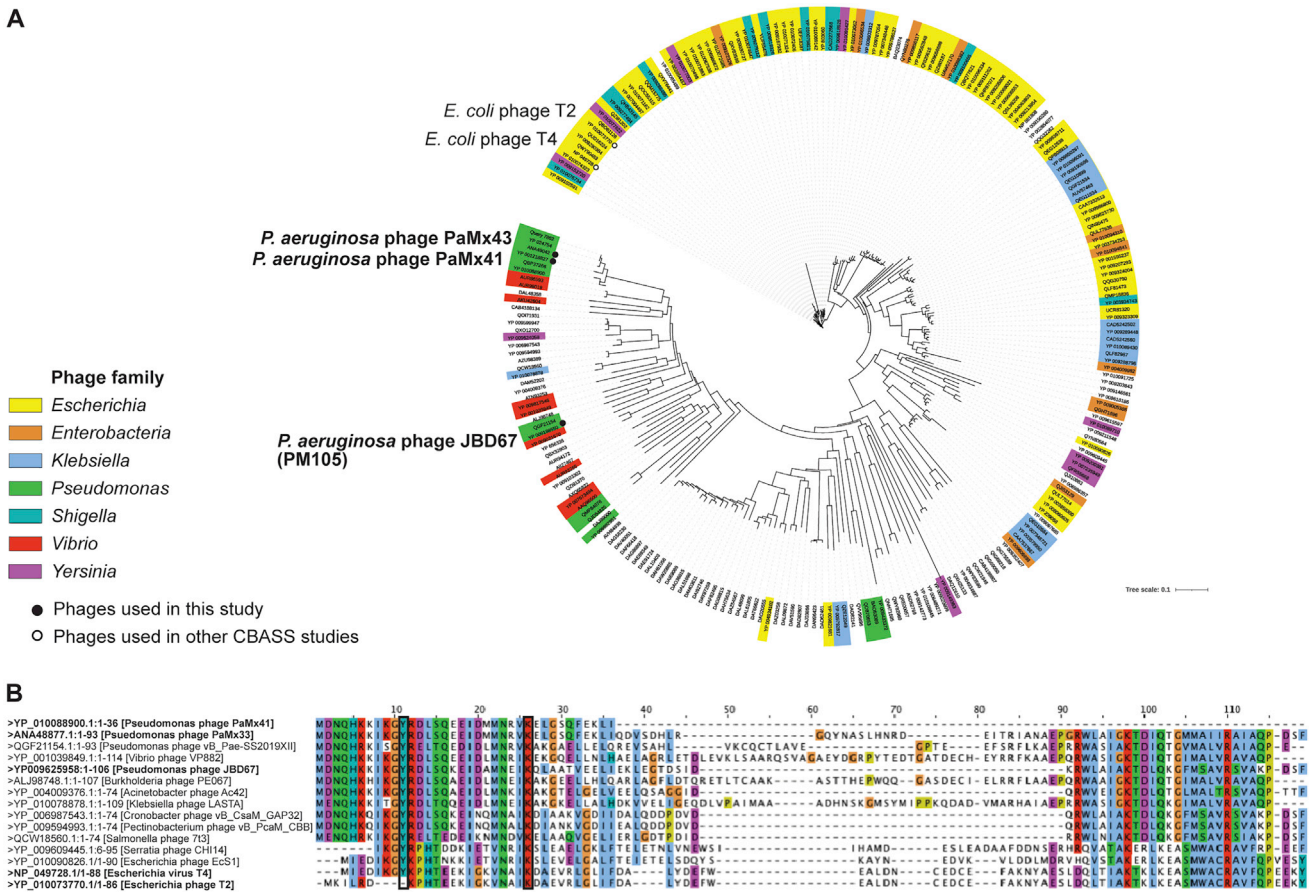

Figure S3. Acb2 is found in a broad diversity of phages and bacteria, related to Figure 2

(A) Phylogenetic tree of *acb2* across the genomes of 239 tailed phages (*Caudovirales*) following two iterations of PSI-BLAST. Phages families that are colored are the most frequently identified. Phages relevant to this study are in bold.

(B) Multiple sequence alignment of PaMx41-*orf24*^{X37Q} Acb2, PaMx33, PaMx43, JDB67 Acb2, and other homologous proteins via MAFFT (multiple alignment using fast Fourier transform) alignment in Jalview. All proteins except T2 and T4 phage homologs were acquired by standard BLASTp, while T2 and T4 were observed on a second round of a PSI-BLAST. Colors indicate an identical amino acid. Black boxes highlight residues Y11 and K26, which are necessary for Acb2 activity.

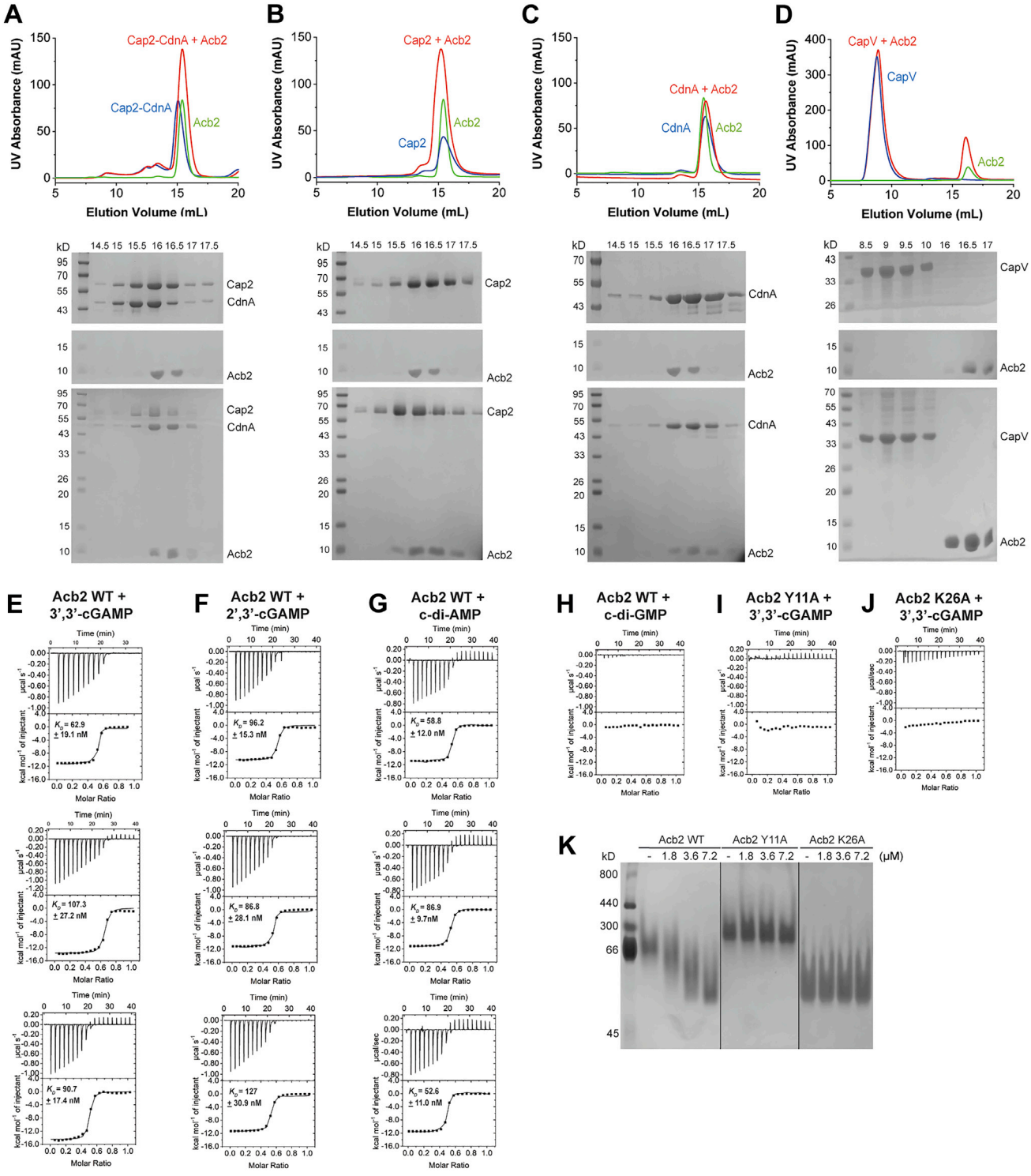

Figure S4. Acb2 does not bind CBASS proteins, but does bind 3′,3′-cGAMP, 2′,3′-cGAMP, and c-di-AMP, related to Figures 3 and 4

(A–D) Gel filtration profile of incubated Acb2 with (A) Cap2-CdnA complex, (B) Cap2, (C) CdnA, or (D) CapV (Superdex-200 increase 10/300 GL, GE Healthcare).

(E) ITC assays to test binding of 3′,3′-cGAMP to Acb2 WT.

(F) ITC assays to test binding of 2′,3′-cGAMP to Acb2.

(legend continued on next page)

(G) ITC assays to test binding of c-di-AMP to Acb2 WT.
(H) ITC assay to test binding of c-di-GMP to Acb2.
(I and J) ITC assay to test binding of 3′,3′-cGAMP to Acb2 Y11A and K26A, respectively.
(K) Acb2 and its mutants were incubated with 3′,3′′-cGAMP at indicated concentrations. Then the samples were subjected to native PAGE.

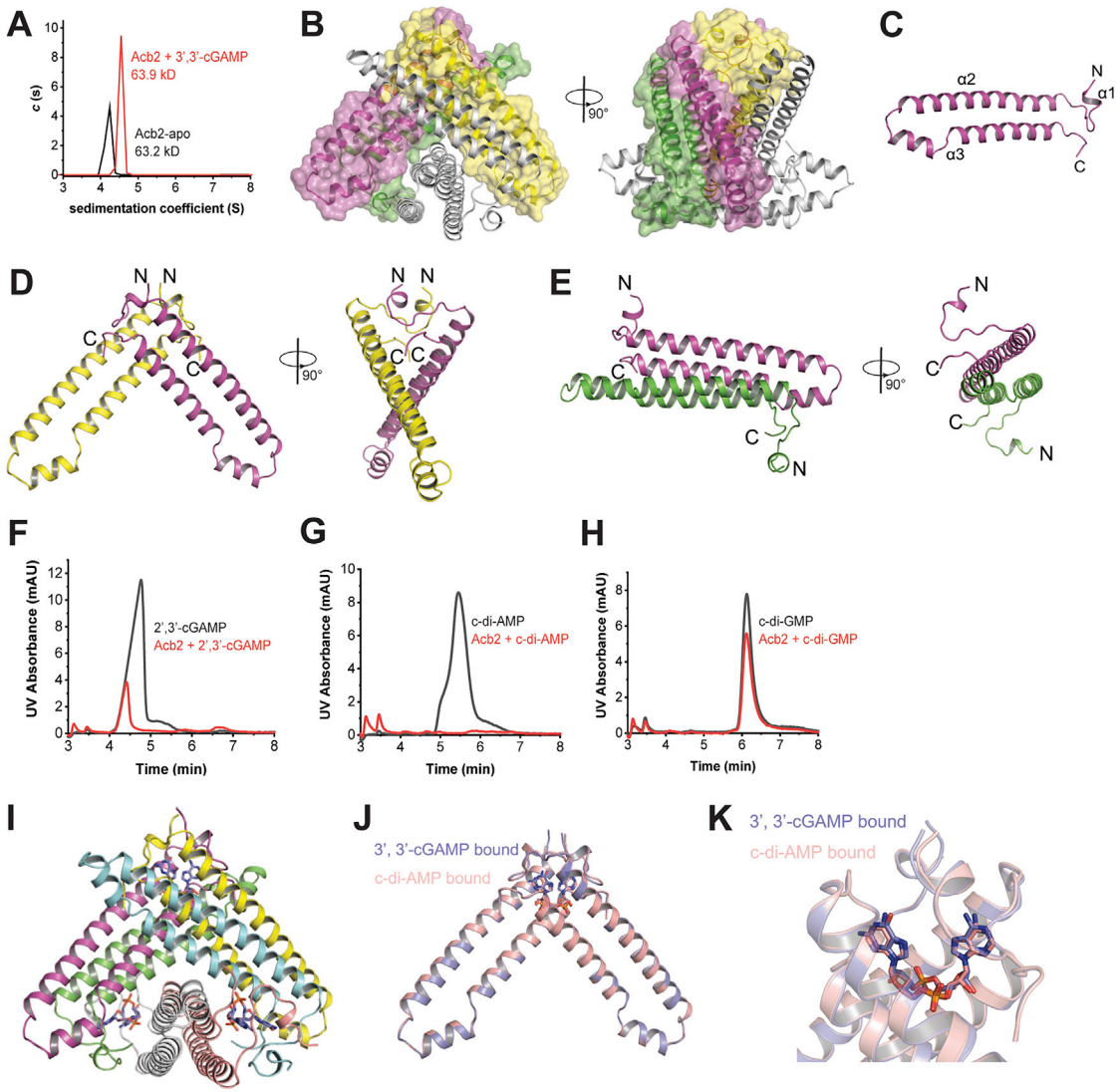

Figure S5. Structures of apo and dinucleotide bound Acb2, related to Figure 4

(A) Analytical ultracentrifugation (AUC) analysis of Acb2 and its complex with 3′,3′-cGAMP.

(B) Structure of the Acb2 hexamer.

(C) Structure of the Acb2 monomer.

(D and E) Two types of dimer of protomers as in (B) are shown.

(F–H) The ability of Acb2 to bind 2′,3′-cGAMP/c-di-AMP/c-di-GMP was analyzed by HPLC. 2′,3′-cGAMP/c-di-AMP/c-di-GMP standards were used as a control. The remaining cyclic dinucleotides after incubation with Acb2 were tested.

(I) Overall structure of Acb2 bound with c-di-AMP.

(J and K) Structural comparison between an Acb2 dimer in c-di-AMP-bound form (colored in pink) and 3′,3′-cGAMP-bound form (colored in slate).

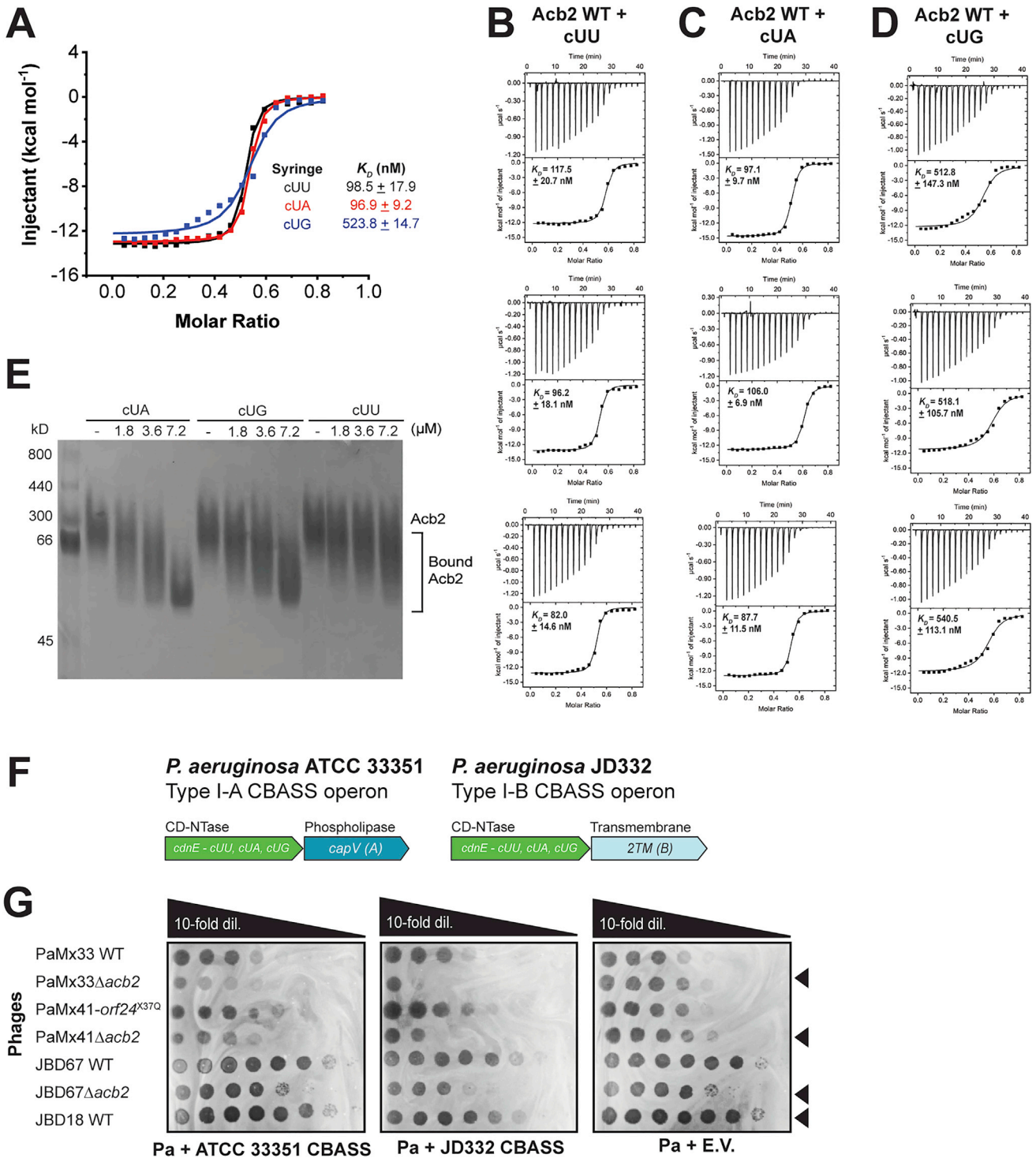

Figure S6. Acb2 binds to the predicted CdnE cyclic dinucleotide products and protects phages against type I-A and type I-B CBASS immunity that encode CdnE cyclase, related to Figure 3

(A–D) (A) Isothermal titration calorimetry (ITC) assays to test binding of cyclic dinucleotides to Acb2. cUU, cUA, and cUG represent 3′,3′-cyclic-di-UMP, 3′,3′-cyclic-UMP-AMP, and 3′,3′-cyclic-UMP-GMP, respectively. Representative binding curves and binding affinities are shown. The K_D values are mean ± SD (n = 3). Raw data for these curves are shown in (B)–(D).

(E) Native PAGE showed the binding of Acb2 to cyclic dinucleotides.

(legend continued on next page)

(F) *P. aeruginosa* ATCC 33351 and JD332 CBASS operons with predicted cyclic dinucleotides.[7]

(G) Plaque assays with the indicated phages spotted in 10-fold serial dilutions on a lawn of *P. aeruginosa* cells (PAO1), which naturally lacks CBASS, over-expressing a CBASS operon or empty vector (E.V.); clearings represent phage replication. Black arrowhead highlights change in phage titer specific to phages lacking *acb2*.

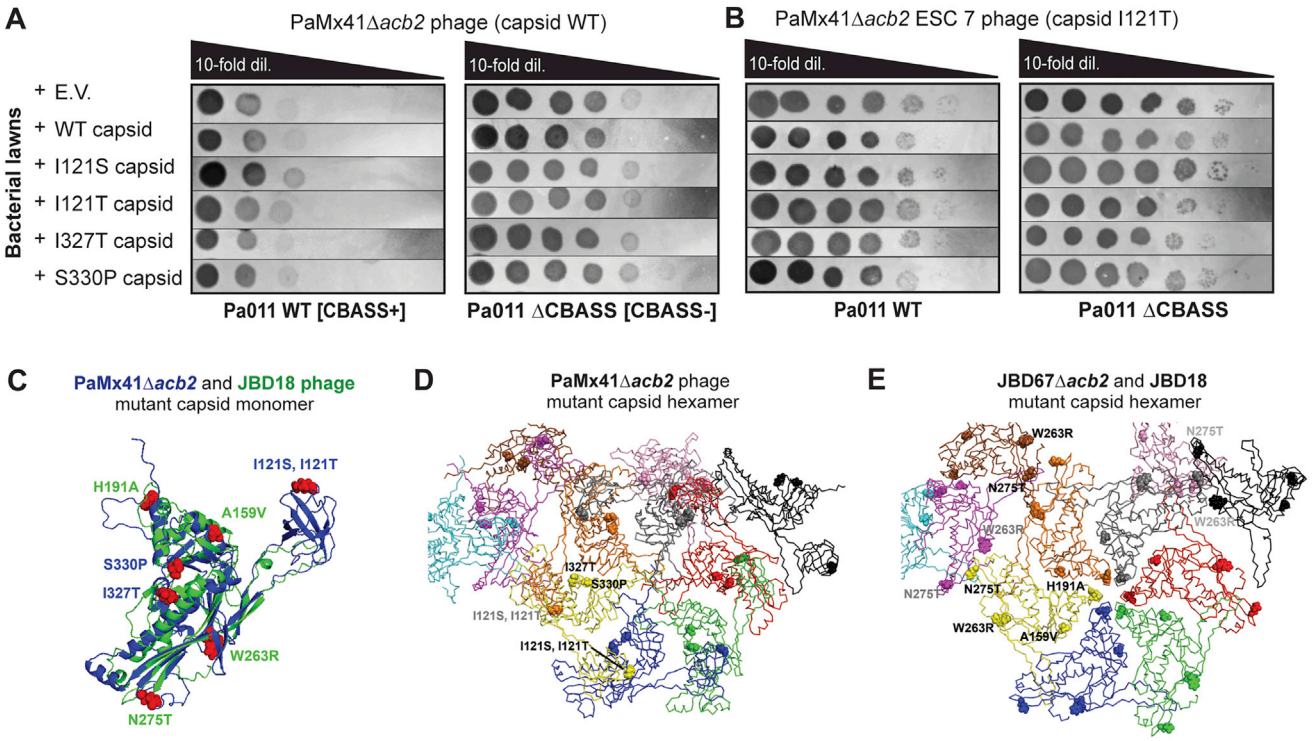

Figure S7. PaMx41 phage remains sensitive to CBASS immunity in the presence of major capsid escape allele expression, related to Figure 5

(A) Plaque assays were performed with PaMx41Δ*acb2* phage, harboring a wild-type (WT) capsid, spotted in 10-fold serial dilutions on a lawn of Pa011 WT [CBASS+] or ΔCBASS [CBASS−] overexpressing the indicated genes; clearings represent phage replication.

(B) Plaque assays were performed with PaMx41Δ*acb2* CBASS Escaper phage 7, harboring a mutant (I121T) capsid, spotted in 10-fold serial dilutions on a lawn of Pa011 WT or ΔCBASS.

(C) Alphafold2 prediction of the PaMx41Δ*acb2* (blue) and JDB18 (green) major capsid protein monomer structures overlaid using PyMOL (RMSD: 4.194). Red spheres represent amino acid residues that are mutated and are labeled with the corresponding aa change.

(D and E) (D) Alphafold2 prediction of the PaMx41Δ*acb2* and (E) JDB18 capsid hexamer structures based on the experimentally solved *E. coli* T4 phage capsid structure (PDB: 6UZC). Spheres represent the aa residues that are mutated. Black and gray colors are indicative of mutations within a capsid monomer and highlight the inter- and intra-protein localization of the mutations.